
Electronic Thesis and Dissertation Repository

8-6-2014 12:00 AM

Evaluating Human Performance for Image-Guided Surgical Tasks

Matthew Kenneth Kramers
The University of Western Ontario

Supervisor

Dr. Roy Eagleson

The University of Western Ontario Joint Supervisor

Dr. Aaron Fenster

The University of Western Ontario

Graduate Program in Biomedical Engineering

A thesis submitted in partial fulfillment of the requirements for the degree in Master of
Engineering Science

© Matthew Kenneth Kramers 2014

Follow this and additional works at: <https://ir.lib.uwo.ca/etd>



Part of the [Bioimaging and Biomedical Optics Commons](#), [Biomedical Commons](#), [Biomedical Devices and Instrumentation Commons](#), [Diagnosis Commons](#), [Medical Education Commons](#), and the [Surgical Procedures, Operative Commons](#)

Recommended Citation

Kramers, Matthew Kenneth, "Evaluating Human Performance for Image-Guided Surgical Tasks" (2014).
Electronic Thesis and Dissertation Repository. 2342.
<https://ir.lib.uwo.ca/etd/2342>

This Dissertation/Thesis is brought to you for free and open access by Scholarship@Western. It has been accepted for inclusion in Electronic Thesis and Dissertation Repository by an authorized administrator of Scholarship@Western. For more information, please contact wlsadmin@uwo.ca.

EVALUATING HUMAN PERFORMANCE FOR IMAGE-GUIDED
SURGICAL TASKS

(Thesis Format: Integrated Article)

by

Matthew Kramers

Graduate Program in Biomedical Engineering

A thesis submitted in partial fulfillment
of the requirements for the degree of
Master of Engineering Sciences

The School of Graduate and Postdoctoral Studies
The University of Western Ontario
London, Ontario, Canada

© Matthew Kramers 2014

Abstract

The following work focuses on the objective evaluation of human performance for two different interventional tasks; targeted prostate biopsy tasks using a tracked biopsy device, and external ventricular drain placement tasks using a mobile-based augmented reality device for visualization and guidance. In both tasks, a human performance methodology was utilized which respects the trade-off between speed and accuracy for users conducting a series of targeting tasks using each device. This work outlines the development and application of performance evaluation methods using these devices, as well as details regarding the implementation of the mobile AR application. It was determined that the Fitts' Law methodology can be applied for evaluation of tasks performed in each surgical scenario, and was sensitive to differentiate performance across a range which spanned experienced and novice users. This methodology is valuable for future development of training modules for these and other medical devices, and can provide details about the underlying characteristics of the devices, and how they can be optimized with respect to human performance.

Keywords

Human performance, image-guided surgery, augmented reality, targeted TRUS-guided prostate biopsy, external ventricular drain placement

Co-Authorship Statement

The following thesis is presented in an integrated article format containing chapters based on the following works that are either published or in preparation for submission:

Chapter 2: Kramers, M., de Ribaupierre, S., Fenster, A. Eagleson, R.: Evaluating Human Performance for Needle Guidance Tasks Using a Prostate Biopsy Device. (In preparation for submission)

My contributions towards this chapter include the development of the modified targeted biopsy user interface that enabled the collection of human performance data from the device originally developed in Aaron Fenster's lab. Aaron Fenster provided me with access to the device used in this study, as well as the assistance via support staff for troubleshooting when problems were encountered. With the guidance of Sandrine de Ribaupierre, Roy Eagleson, and Aaron Fenster, I was able to create and conduct a user experiment in order to collect the necessary data for evaluation. I performed all of the evaluation of performance including the statistical analysis and result validation.

Chapter 3: Kramers, M., Armstrong, R., Bakhshmand, S.M., Fenster, A., de Ribaupierre, S., Eagleson, R.: A Mobile Augmented Reality Application for Image Guidance of Neurosurgical Interventions. American Journal of Biomedical Engineering 2013, 3(6): 169-174

My contributions towards this chapter include the development of the augmented reality application on the mobile platform. Ryan Armstrong provided the details and implementation of the image processing components of the study, allowing for the anatomical surface models to be constructed from CT images and used in the application. Saeed Bakhshmand provided guidance and inspiration for the implementation of the application by contributing a review of existing augmented reality applications in surgery.

Sandrine de Ribaupierre provided the original concept and motivation of the mobile application to potentially assist neurosurgeons. Roy Eagleson provided motivation and guidance with implementation details and contributed feedback during the design process. Aaron Fenster also contributed motivation and guidance for this work.

Chapter 4: Kramers, M, Armstrong R., Bakhshmand, S.M., Fenster A., de Ribaupierre S., Eagleson R.: Evaluation of a mobile augmented reality application for image guidance of neurosurgical interventions. *Studies in Health Technology and Informatics*. 2014; 196:204-8.

My contributions towards this work include the development and implementation of the mobile application. Ryan Armstrong contributed the image processing related components necessary to carry out this work. Saeed Bahkshman provided assistance with constructing and running the experimental setup and data collection. Aaron Fenster provided support and guidance throughout this work. Sandrine de Ribaupierre provided the concept for this work, as well as direction for the experimental design. Roy Eagleson also provided support with the experimental design and original concept and implementation.

Acknowledgments

I would like to thank my supervisors whom both provided the direction and continuous support for this work: Dr. Roy Eagleson who was always available to provide his valuable insight and clever ideas for development and implementation during my final undergraduate project all the way up to the end of my Master's degree, and Dr. Aaron Fenster for his unwavering support and direction throughout my time as a summer research assistant and graduate student. I would like to thank Dr. Sandrine de Ribaupierre for her invaluable clinical and neurosurgical knowledge and expertise and for providing valuable motivation to ensure my work was practical for use in a clinical environment.

I would like to thank all members of both Dr. Eagleson's lab and Dr. Fenster's lab for welcoming me as a colleague and providing me with invaluable experience and knowledge, both academically and practically. I thank Lori Gardi for contributing her time and extensive knowledge of software development as well as her experience with medical device development. I thank Dr. David Tessier for his technical support and research lab experience. I thank Jeremy Cepek for providing me with his engineering experience and wisdom as a fellow graduate student. I would also like to thank Kevin Barker for his extensive knowledge and skills in manufacturing, and for always being willing to help out. I would also like to thank Ryan Armstrong for creating great discussions about software, which was very valuable to my work as a graduate student. I would like to recognize several other members of the lab and other colleagues for their valuable discussions, support, and contributions to my work: Jing Jin, Saeed Bakhshmand, Justin MacKenzie, Shaun Carnegie, Ngan Nguyen, Lauren Allen, Matt Gravett, Tharindu De Silva, Eli Gibson, Hamid Neshat, Jay Baxter, Kamyar Abhari, Jacques Montreuil, Igor Gyackov, Chandima

Edirisinghe, Dr. Derek Cool, Kimberly Booth, Janette Wallace, Debbie Lillie, Christine Ellwood, as well as any other members that helped me during my graduate studies.

I would like to thank my examination committee for their invaluable time spent reviewing and evaluating my work: Dr. Terry Peters, Dr. Aaron Ward, and Dr. Luiz Capretz – I really appreciate your help.

Finally, I would like to thank the many people outside of the lab that contributed support and friendship throughout my time as a graduate student. My loving girlfriend Ashley D'Andrea who always provides support and keeps me positive. My parents, Ken and Lynda, who have forever supported me and have shaped me into the person I am today. My brother Jordan who has always served as a role model for achieving success and happiness. And of course my friends with whom I've shared countless good times: Jacob Hoefnagels, Josh Douwes, Kyle Rosso, Christian Moulton, Tyler Savoie, Scott Haig, Mike Byers, Justin Beland, Rachel Farkas, Peter Martin, Kathryn Manning, and everyone else – you know who you are.

I would also like to acknowledge the sources of funding including the NSERC CREATE Computer-Assisted Medical Interventions Scholarship, and Western Graduate Research Scholarship.

Table of Contents

Abstract.....	ii
Co-Authorship Statement.....	iii
Acknowledgments.....	v
Table of Contents.....	vii
List of Tables.....	x
List of Figures.....	xi
List of Appendices.....	xiii
1. Introduction.....	1
1.1 Prostate Cancer: Disease and Diagnosis Techniques.....	1
1.1.1 Diagnosis	2
1.2 External Ventricular Drain Insertion †	9
1.3 Augmented Reality.....	10
1.3.1 Tracking Techniques.....	11
1.3.2 Display Platforms and Devices.....	13
1.3.3 Visualization Techniques.....	15
1.3.4 Augmented Reality in Medicine and Surgery	17
1.4 Human Performance: Theory, Application	19
1.4.1 Fitts' Law.....	19
1.4.2 Application	22
1.4.3 Additional Performance Evaluation Methods.....	23
References.....	24
2. Evaluating Human Performance for Needle Guidance Tasks Using a Prostate Biopsy Device†.....	33
2.1 Introduction	33
2.2 Modeling Image-Guided Human Performance	35
2.3 Methods.....	37
2.3.1 Prostate Biopsy Device.....	37
2.3.2 Targeting Task Design	38

2.3.3	Participants and Experimental Procedure	40
2.3.4	Hypothesis.....	41
2.4	Results.....	42
2.5	Discussion.....	45
2.6	Conclusion	47
	References.....	48
3.	A Mobile Augmented Reality Application for Image Guidance of Neurosurgical Interventions [†]	50
3.1	Related Work.....	50
3.2	Methods.....	52
3.2.1	Vuforia and Augmented Reality Implementation.....	52
3.2.2	Segmentation and Registration of Patient Data	55
3.2.3	User Controlled Registration Correction	59
3.2.4	Evaluation of System Accuracy	60
3.3	Results.....	61
3.4	Discussion.....	61
3.5	Conclusion	62
3.6	Acknowledgment.....	62
	References.....	62
4.	Evaluation of a Mobile Augmented Reality Application for Image Guidance of Neurosurgical Interventions [†]	65
4.1	Introduction	65
4.2	Methods.....	65
4.3	Evaluation	68
4.4	Results.....	69
4.5	Conclusion	70
	References.....	71
5.	Conclusion	73
	Appendix A: Additional Experiments.....	1
	Appendix B: Software Design and Architecture	4

Appendix C: Supplementary Data	8
Appendix D: Supplementary Images.....	10
Appendix E: Permissions	12
Curriculum Vitae	13

List of Tables

Table 2-1: Target Distance and Tolerance Configuration Parameters.....	39
Table 2-2: Performance results for all users without adjustments to accuracy	43
Table 2-3: Performance results for all users with accuracy adjustments applied	44
Table 2-4: Sum of variance vs. target distance	47
Table 3-1: Targeting error measured as the Euclidean distance between targeted corner location and actual corner location	61
Table 4-1: Average Intra-User Deviation from Target [mm]	69
Table 4-2: Average Inter-User Deviation from Target [mm]	70
Table 4-3: Average pointing time [s]	70

List of Figures

Figure 2-1: Biopsy procedure schematic with TRUS probe inserted into the patient's rectum along with needle aligned in parallel to the ultrasound image plane	34
Figure 2-2: User Interface for visualization of biopsy needle and targets and Prostate Biopsy Device for performing targeting tasks	38
Figure 2-3: Isometric view of all target configurations and approach angles distributed on a sphere (left) and from users' viewpoint along the z-axis.....	40
Figure 2-4: Fitts' Law profile and regression line for a single user for a total of 216 task configurations.....	43
Figure 2-5: Tangential velocity profiles for all users averaged and normalized for each target condition.	45
Figure 2-6: Tangential velocity profiles sorted by target distance (solid) and variance of each trajectory for all users (dotted)	47
Figure 3-1: Tracking marker fixed to safety glasses for patient head pose estimation and registration of anatomy to scene.....	54
Figure 3-2: The tracked pointing device provides visual feedback for planning entry point locations and trajectories. The device also allows for additional interaction between the user and the AR scene.	55
Figure 3-3: Anatomy segmented from preoperative images aligns with the physical tracker and is positioned using the nasion as a positional landmark.	58

Figure 3-4: Users have access to multiple sliders and buttons to manually adjust the virtual models to achieve appropriate alignment of anatomy, as well as visual settings that aid in guidance..... 59

Figure 4-1: Glasses with attached tracking marker..... 66

Figure 4-2: User viewing ventricular anatomy through device 67

List of Appendices

Appendix A: Additional Experiments	1
Appendix B: Software Design and Architecture	4
Appendix C: Supplementary Data	8
Appendix D: Supplementary Images	10
Appendix E: Permissions	12

Chapter 1

1. Introduction

This work focuses on the objective evaluation of human performance for two specific surgical tasks. The first task involves a device that is used for performing targeted TRUS-guided biopsy of the prostate. Due to high prevalence of prostate cancer in men, the targeted biopsy procedure is becoming an increasingly desirable method of diagnosing cancer in men. For this reason, we proposed a method for the objective evaluation of users using a particular targeted biopsy device. The results obtained in this work can be used towards further optimization of the device towards more efficient user performance. The second surgical task focuses on the neurosurgical procedure of placing an external ventricular drain. This procedure is often performed free-hand and by novice surgeons, and is therefore susceptible to human targeting errors and consequential complications to the patient. The following work highlights the development of a mobile-based augmented reality device that enables users to visualize and perceive the target location within the lateral ventricles of the brain by providing the view of pre-operative 3D scans overlaid in Augmented and Virtual Reality presentation to overlay in the context of the view of the patient's head. In addition to a description of this development, human performance data was also collected for users operating the device and performing target and trajectory estimation tasks. The following section outlines relevant literature in prostate cancer diagnosis, the external ventricular drain insertions procedure, augmented reality with a focus on surgical applications, as well as human performance evaluation

1.1 Prostate Cancer: Disease and Diagnosis Techniques

Prostate cancer is the most common form of cancer found in men in North America, with an estimated 23,600 new cases in Canada alone during the

year 2013 [1]. This equates to an approximate probability of 14.3% of men, or 1 in 7, to develop prostate cancer in his lifetime. It is estimated that a total of 3,900 men will die as a result of prostate cancer in the year 2013 [2]. In addition to premature death as a result of this disease, there are significant impacts upon the health-related quality of life (HRQOL). In a study comparing the impact on HRQOL for men before and after prostate cancer diagnosis with a control group, Reeve *et al.* found that there was a significant decline in both the physical and mental health of a patient within the first 6 months of diagnosis compared to the control group [3]. In addition, certain social aspects of the patient's life were noted to also suffer as a result of diagnosis. Although this particular study was limited to patients above the age of 65 years, it is reasonable to assume that prostate cancer diagnosis has a significant impact on younger men [4]. In addition, many of the therapies that exist to treat prostate cancer have an increased likelihood of increasing the chance for complications that can result in urinary, bowel and sexual health issues [5]. This due to the close proximity of the patient's rectum, bladder, urethra, and neurovascular bundles with the prostate. One particular instance of such treatment is the radical prostatectomy procedure which is often detrimental to urinary function [6].

1.1.1 **Diagnosis**

There are four methods that are most commonly used to diagnose prostate cancer: prostate specific antigen (PSA) test, digital rectal examination (DRE), imaging, and prostate biopsy. The following section describes each of the stated diagnostic methods for detecting and characterizing prostate cancer in men, with a focus on targeted biopsy.

1.1.1.1 **Prostate Specific Antigen Test**

Prostate specific antigen (PSA) is a protein that is secreted by epithelial cells of the prostate gland. A study performed by [7] showed that there was a

correlation between the level of PSA in a patient's blood and the stage of the cancer. In addition, a relationship between the PSA levels and the estimated volume of the tumour was also determined and reported by [8]. The increase in PSA levels detected in the bloodstream has been attributed to the disturbance of the prostate glandular structure due to the presence of cancer [9]. Although this discovery was a significant step towards more effective prostate cancer diagnosis, there is much debate over the value of such screening methods, since it often results in overdiagnosis, and consequently overtreatment of the disease, which may be undesirable for men with slowly progressing cancer.

1.1.1.2 **Digital Rectal Examination**

The digital rectal examination (DRE) is a method for cancer detection where a physician uses a finger to palpate the prostate through the patient's rectum. This diagnostic examination is sensitive to cancer contained in the peripheral zone (PZ) of the prostate, as this area is located adjacent to the rectal wall. The physician attempts to detect hardened areas of the prostate tissue which may indicate the presence of cancer, often indicated by asymmetric tissue stiffness across the left and right lobes of the prostate. The result of the DRE is typically used in conjunction with the detected PSA levels in a patient's blood to determine the risk and/or presence of prostate cancer. However, in patients with low PSA levels (< 4.0 ng/ml), the DRE has a low positive predictive value (PPV), and therefore the DRE alone is not a reliable predictor in all patients. Furthermore, the DRE is prone to missing areas of the prostate outside of the PZ, and therefore must be accompanied by alternative diagnostic tests to accurately identify the presence of prostate cancer.

1.1.1.3 **Prostate Imaging**

The following section provides a brief overview of the most commonly used and state-of-the-art prostate cancer imaging modalities. Although there are many modalities used in relation to prostate cancer, including computed tomography (CT), positron emission tomography (PET), and others, this section is limited to ultrasound (US) and magnetic resonance (MR) imaging techniques. The former modalities (PET, CT, etc.) are typically used in the evaluation of metastases and/or lymph node analysis, and therefore will not be discussed in the following section.

1.1.1.3.1 **Ultrasound**

Ultrasound provides many advantages over MR imaging for prostate cancer imaging. Ultrasound provides real-time image sequences, allowing it to be useful intra-operatively during procedures such as prostate biopsy or brachytherapy [10, 11]. Furthermore, ultrasound has been used to obtain prostate volume information, which is necessary for determining PSA density [10]. In addition, the low cost of ultrasound devices allow for greater access in many hospitals over MR imaging, which is both expensive and physically large.

Although ultrasound provides some clear advantages, it is not without its trade-offs. For instance, ultrasound is typically only sensitive to large, higher grade tumour volumes as noted by [12]. In addition, ultrasound is not typically sensitive to tumors located in the transition zone of the prostate, which can contain around 20% of prostate cancer [13].

1.1.1.3.2 **Magnetic Resonance Imaging**

In a review performed by Hricak *et al.* it was demonstrated that magnetic resonance imaging (MRI) has the potential for efficiently detecting and localizing prostate cancer [10]. There is growing evidence that suggests this

to be possible from the improvement in MR performance with combined modern multiparametric MRI (mpMRI) techniques, such as T1- and T2-weighted images, dynamic contrast, diffusion weighting, and proton spectroscopy [14, 15]. Despite this fact, there is much debate in the professional community over the accuracy and clinical usefulness of such techniques stemming from the variability in quality and methodology of reported studies in the field [16]. To address these issues, Dickinson *et al* conducted a meeting with 16 European prostate cancer experts to determine a set of recommendations towards a standardized method for interpreting and reporting of prostate mpMRI for prostate cancer detection and localization [17]. Despite the variability present in the literature, the use of MRI in the clinical setting is certainly promising, especially for determining optimal targets for targeted biopsy in men whom are suspected to have cancer [18].

1.1.1.4 **Biopsy**

A biopsy of the prostate involves the insertion of specialized needles into the prostate to obtain small tissue samples of the prostate tissue for pathological analysis. The collected samples, also called biopsy cores, are then prepared for further examination under a microscope by a pathologist. A pathologist observes the appearance and structure of the glands and the cells that compose them, and is able to determine if the tissue is cancerous as well as grade the aggressiveness of the identified cancer. The Gleason grading system is used to rate the cancer in all obtained biopsy cores. Although this grading system has become a significant tool for the estimation of the prognosis of prostate cancer in a patient (it is currently considered as the gold standard method for grading cancer [19]), there is still a potential for errors inherent in the prostate biopsy procedure that can contribute to unreliable estimates of the total prostate's burden and/or aggressiveness of the cancer [20], despite the accuracy of the pathologist.

1.1.1.4.1 **Transrectal Ultrasound (TRUS)-Guided Biopsy**

The transrectal ultrasound-guided biopsy (TRUS-GB) procedure is currently the most commonly used method for obtaining biopsy cores for the purpose of diagnosing prostate cancer in men. In this approach, the patient is positioned in a lateral decubitus position (lying down on the side) and an ultrasound probe is inserted through the patient's rectum allowing the physician to visualize the prostate and biopsy needles via ultrasound through the rectal wall. The needles are directed through a needle guide that is attached to the ultrasound probe, such that they can be visualized on an external display. The physician directs these needles to regions within the prostate that are known to have a high incidence of developing prostate cancer and proceeds to collect multiple biopsy cores. Approximately 75% of prostate cancers are found in the peripheral zone (PZ) and as a result, the initial round of biopsies is typically directed at this region. Recently the standard number of biopsy cores collected during a procedure increased from 6 (sextant) to 10-12. This increase is attributed to the result demonstrated in [21] that reveals that in up to 1 in 3 cases the sextant biopsy configuration will underestimate the reported Gleason grade. Although the increased number of biopsy cores collected increases the likelihood of detecting cancer, it also increases the potential symptoms occurring after biopsy procedure, including urinary retention, sepsis and dysuria [22]. Furthermore, the anterior, midline and apex regions of the prostate are difficult to perform a biopsy using the TRUS-GB approach due to their physical locations with respect to surrounding anatomy [23]. The TRUS-GB procedure has potential for delivering an accurate diagnosis of prostate cancer, and recent developments in imaging have gained the targeted biopsy method attention among physicians.

Upon an initial negative biopsy of the prostate, there remains a chance that cancer is still present in the prostate. It is therefore common practice to perform a repeat biopsy procedure to collect additional biopsy cores for

analysis. The repeated biopsy not only increases the patient's discomfort and the potential for undesirable side-effects, but it has been shown that the repeat biopsy is no more sensitive to detecting cancer than the initial biopsy [24]. Although the physician attempts to obtain biopsy cores from areas that were not sampled in the initial or previous biopsy, there is no guarantee that regions are not resampled. Both groups in [24, 25] showed that the detection rate of a repeated biopsy after an negative first biopsy was in the range of 10-20%, indicating that repeat biopsies have poor sensitivity for cancer detection in certain patients.

1.1.1.4.2 **Targeted Biopsy**

To accommodate some of the sensitivity issues with TRUS-GB procedures, there has been growing interest in incorporating magnetic resonance images (MRI) to provide specific targets for biopsy, as well as using such images for detection, localization and grading of the cancer [26]. By incorporating the location of suspicious areas into the biopsy procedure, and ensuring that those areas are sampled, the probability of detecting cancer potentially increases and the number of subsequent biopsies decreases, resulting in a decrease of the accompanying side-effects of the biopsy procedure. By consequence, the accuracy of the Gleason score obtained from the biopsy can be therefore increased by using targeted biopsy [23]. This becomes important when determining therapeutic treatment options, since each treatment method has different associated side effects [21].

The targeted biopsy method has been evaluated with respect to diagnostic outcomes and clinical utility. Two studies determined that that targets deemed as being suspicious for cancer on MRI had an estimated prevalence of 63% when an MRI was acquired preceding the biopsy [27, 28]. This result is promising and has potential to improve the outcome of biopsy procedures. Several other studies concluded that there was an average probability of 36%

for detecting cancer using standard systematic biopsy, and a 48% probability for detecting cancer using the target biopsy approach [23]. It was also determined that 30% of targeted biopsy cores contained cancer, while only 7% did while using the non-targeted approach. Therefore it can be concluded that less biopsy cores are required to detect cancer using the targeted biopsy method.

1.1.1.4.3 **Targeted Biopsy Devices**

As a result of the increasing interest in targeted biopsy of the prostate, several groups have developed systems that promote improved diagnosis of cancer through the inclusion of techniques such as tracked US and in-bore MR guided devices. Bax *et al.* [24] developed a passive mechanical device that utilized existing 2D ultrasound equipment used for biopsy to allow physicians to perform biopsies at predetermine locations with high accuracy. This functionality is valuable, allowing for locations in the prostate to be re-biopsied if needed, as well as for enabling the precise recording of sampled locations during systematic biopsies. In addition, there is opportunity for such tracked devices to use image fusion with other image modalities, such as MRI, which can further assist the physician with planning the procedure. Other groups have developed similar devices that have showed promising results towards optimizing the efficiency of the targeted prostate biopsy procedure and consequently improving the efficiency of cancer diagnosis overall [29, 30]

1.2 External Ventricular Drain Insertion †

Placing an external ventricular drain (EVD) is a fundamental neurosurgical procedure performed to treat acute hydrocephalus – a condition characterized by an accumulation of cerebrospinal fluid within the ventricular system, either due to obstruction or by a problem of reabsorption [31, 32]. The procedure consists of drilling a burr-hole in the skull, followed by a blind placement of an external ventricular drain using external landmarks for guidance. This procedure allows drainage of cerebrospinal fluid to relieve intracranial pressure. While most neurosurgical interventions are usually performed in an operating room (OR) while the patient is under sedation [33], this is rarely the case for this procedure. Since the insertion of an EVD is usually performed on critically ill patients (either for acute hydrocephalus or after a trauma), the predominant difficulty involves transportation of the patient [34] mostly due to life-support equipment [35]. To accommodate such a scenario, manual operation of mobile drills for burr-hole trephine can be performed within the Intensive Care Unit or in the Emergency room. While advantageous in avoiding the difficulties in relocation to the OR, this technique precludes the use of certain immobile equipment present within the OR.

While external ventricular drain placements are among the most common and basic of neurosurgical procedures, they are generally performed free-hand, relying on surface landmarks on the patient as well as the spatial reasoning of the operating surgeon to determine optimal trajectory of tools within the complex workspace. While it might be relatively easy to target large ventricles placed in a normal anatomical position, most patients will

†.Kramers, M., Armstrong, R., Bakhshmand, S.M., Fenster, A., de Ribaupierre, S., Eagleson, R., A Mobile Augmented Reality Application for Image Guidance of Neurosurgical Interventions. American Journal of Biomedical Engineering 2013, 3(6): 169-174

have small ventricles with some anatomical variation, possibly displaced by lesions occurring after the trauma. As a result of navigational error due to free-hand placement, a number of complications can occur, including malposition, non-function, infection and haemorrhage [36]. While neurosurgeons generally consider the manual procedure to be safe, a number of studies have identified the technique as suboptimal [37-39]. In addition, this procedure is often performed by junior residents who are on-call. Indeed, many of these complications are a result navigational error, often requiring repositioning of the EVD into the ventricular system. In addition to the complications resulting from such misplacements, the procedure time is increased and additional, un-necessary tissue damage occurs.

1.3 **Augmented Reality**

Augmented reality (AR) is a form of virtual reality that combines the physical, real-world environment with computer generated elements, such as video and graphics. In a definition provided by Azuma *et al.* [40], AR is described as system that can perform the following tasks:

- Combines real and virtual imagery
- Be capable of interaction in real-time
- Be able to perform 3D registration of virtual objects within the real-world scene

While using AR, a user's visual perception can be altered, such that virtual objects appear to be part of the real physical scene. By providing a means of interaction with the scene, the AR system can provide additional visuospatial information to the user through visual cues such as lighting and motion parallax. This capability is advantageous in surgery, since it enables the visualization of medical images and anatomical surface models in a more natural way. This approach attempts to minimize the cognitive load faced by a surgeon, who is typically required to mentally reconstruct the images from 2-D, slice-based, images displayed on an external monitor.

The following section discusses different devices and methods for providing users with an immersive AR experience, followed by an overview of several tracking techniques employed in AR. Finally, several existing mobile AR devices aimed towards assisting surgeons will be reviewed.

1.3.1 **Tracking Techniques**

In a review performed by Zhou *et al.*, it was determined that research directed towards tracking technology in AR was the most popular topic for participants of several AR focused conferences over the last decade [41]. The following section outlines the three main categories of tracking technologies, and their application and feasibility in a surgical environment.

1.3.1.1 **Sensor-Based Tracking Techniques**

Sensor-based tracking involves the use of sensors in order to provide the information necessary for effective AR. These sensors employ technology based on magnetic, acoustic, inertial, optical, and/or mechanical technologies. Although each of the sensor technologies are capable providing sufficient AR tracking, each implementation comes with its own set of trade-offs. For instance: optical (infrared) tracking is capable of providing high tracking accuracy in six degrees of freedom (6DOF), however, it requires the cameras used to have continuous line of sight, as well as the necessity of physically attaching markers to the object of interest [42]. In a surgical environment, these requirements may be difficult to satisfy due to the number of people within the operating room, as well as the space requirements needed for existing surgical equipment. In addition, the footprint of such optical tracking systems may not be feasible in certain operating rooms. Magnetic tracking may provide accurate and fast tracking for AR; however the presence of ferromagnetic materials can significantly degrade the tracking accuracy of the system. In a study performed by Milne *et al.*, it was found that mild steel produced a significant tracking error in both the translation and rotation

components when magnetic tracking was used [43]. Since many elements of the surgical environment may contain these materials, this type of tracking may be difficult to accommodate. In the case of mechanically tracked AR system, such as the first head-mounted display (HMD) AR device by Sutherland *et al.* [44], user interaction may be restricted due to the fixed nature of the device. As a result, this may lead to limited mobility of the surgeon, which is disadvantageous.

1.3.1.2 Vision-Based Tracking Techniques

The use of image processing based methods to extract camera pose information was noted as being the most active area within AR tracking research [41]. This type of tracking can be divided into two categories: feature based and model based [45]. Feature based tracking uses the minimization of the distance between features extracted from a 2-D image and projected 3-D object features to determine the camera pose [46]. Some particular feature-based tracking methods use methods such as Harris feature detection along with the random sample consensus (RANSAC) algorithm to match the detected features with a known configuration [47]. In recent work by Pilet, the tracking non-rigid (non-planar) surface markers were achieved using advanced featuring detection and matching techniques. In addition, there is a growing trend towards using marker-less tracking by detecting natural features within the scene, such as lines and edges [48-51]. Methods that employ marker-less tracking offer many advantages, despite the associated computational cost. One particular method of natural feature detection, present by Park *et al.* demonstrated the tracking robustness of initially registering the AR device with known features, and then constantly accumulating natural features in order to correct the registration even after the original marker is out of sight [52]. These natural feature tracking techniques utilize the relative ease of discerning edges from images, which are also robust to lighting changes within the real world scene. Some

researchers have further explored natural feature tracking methods by incorporating gradient and texture information observed in the scene [53].

1.3.1.3 **Hybrid Tracking Techniques**

There are some specific instances where features of each of the above methods of tracking are desirable, and therefore some researchers have explored the application of a combination of sensor- and vision-based techniques to achieve AR tracking. For example, vision-based tracking has low jitter and no drift but requires extensive computation and therefore can be slower than some of the sensor-based approaches. In addition, quick movements of the camera may result in a disruption in the AR scene since the vision-based algorithms are not robust to such drastic changes in its input. Inertial tracking can act to compliment vision-based techniques, by providing motion prediction information to the tracking algorithms and therefore strengthen the overall accuracy of the system [54, 55]. It has been reported that the hybrid tracking approach is the most favorable method of providing tracking information to the AR scene [56].

1.3.2 **Display Platforms and Devices**

With respect to augmented reality in surgery, there are three primary categories of display methods that have been adopted: Video see-through displays, optical see-through displays and projective displays [57]. Each of these methods uses one of following display device types to present virtual objects to the user: Head worn displays, hand-held displays and spatial displays. Each of these device types and display methods is discussed in the following section.

1.3.2.1 **Video See-Through Displays**

Video see-through displays utilize a screen to display a video of the real-world scene with virtual objects augmented within it. This type of display is often

the most inexpensive solution for providing users with AR, and in turn often tends to be the easiest to implement and most readily available. One particular advantage of video see-through displays over alternative technologies is that the brightness and contrast of the virtual objects can be adjusted such that the objects blend into the scene more naturally [58]. One drawback of this type of display is that it is limited by the screen's resolution, which for head-mounted displays can be low. In addition, some implementations provide users with a limited field of view, although this can be addressed by simply increasing the size of the display, if possible. Depending on the position of the display relative to the user, especially in head-mounted setups, video see-through displays may cause disorientation for the user caused by the eye-offset, which requires the user to adjust their perception of the scene [59]. Another disadvantage of head-mounted video see-through displays is that, depending on the ocular configuration, it may cause the user to experience eye strain and fatigue, which may constrain the effectiveness of AR [60].

1.3.2.2 **Optical See-Through Displays**

The optical see-through approach involves combining computer graphics with the actual view of the real world. In this approach, a special mirror is constructed that allows virtual objects to be projected upon the user's field of view, and may be worn by surgeon [61] or can be fixed upon a patient's bed between the surgeon and the patient [62]. Optical see-through head-mounted displays provide users with a lesser sense of immersion within the augmented scene than with the video see-through approach. In addition, since the augmented elements appear on a 2-D plane in front of the real scene, there are more requirements for the surgeon to perform additional visual processing in order to fully obtain the visuospatial information provided by AR. In addition, virtual objects displayed using the optical see-through method may suffer from a lack of brightness and contrast, and have

difficulties portraying occlusion, although some researchers have found ways around this [63]. Despite these disadvantages, the optical see-through method permit more control of the surgeon in an emergency situation, as they have direct view of the patient and operating site and have a higher chance of recognizing misalignment between the scene and the augmented elements [64].

1.3.2.3 **Projective Displays**

The final primary display technology involves the use of projectors to project virtual objects onto target surfaces. This method is advantageous since it does not require any additional eye wear for the user. In addition, projection alleviates the need for the user to focus their eyes, since the virtual objects do not appear directly in front of their eyes, like in head mounted approaches. This method does, however, require additional input devices to allow for user interaction and registration within the augmented scene. In addition, projectors require recalibration for every instance that the target moves, which may be difficult to achieve in dynamic settings. Fortunately, there are methods for automated projector calibration that have the potential to alleviate this issue [65].

1.3.3 **Visualization Techniques**

Visualization systems are essential to image guided medical interventions. Generally, such systems are used to incorporate preoperative information into the surgery. The data used is usually derived from volumetric medical images, such as CT and MR scans, although other preoperative information can also be used, such as surgeon-defined navigational paths and annotations. The overall goal of such a system is to provide the operating surgeon with additional information to better perform a task. In many applications, particularly in minimally invasive surgical techniques, the goal is to provide the surgeon with a window into the inner anatomy of a patient

when the view of target anatomical features is obstructed. With an augmented reality environment, such internal information can be overlaid onto the patient from the perspective of the operating surgeon, providing context for the task that is otherwise unavailable. While clinicians are familiar with slice-based, two-dimensional views of the imaging data, the spatial reasoning required in mentally reconstructing the scene using these techniques increases cognitive load, which may slow the task and inject error [66]. For these reasons, Traub et al. proposed a hybrid navigation interface that combines the both slice-based approach with the in-situ augmented visualization [67]. By subjecting different surgeons with varying experience levels to each of the different combinations of slice-based and volume rendering visualization strategies, a comparison of task completion time and accuracy was made. It was found that overall performance was largely determined by the individual surgeon's experience with each visualization method. However, it was shown that the hybrid visualization approach improved the surgeon's accuracy when compared to in-situ visualization methods, and also improved speed when compared to standard, slice-based visualization. Therefore, it is important to consider the method of visualization within the augmented reality scene and measure surgeon performance to find the optimal means of visualization.

In general, there are two ways to visualize spatial structures deriving from volumetric medical images: isosurface rendering and direct volume rendering (DVR) [68]. DVR allows for the visualization of desired structures directly from the raw medical volume (or with minimal pre-processing). There are numerous algorithms for DVR, which usually involve classification of image voxels based on intensity, position and local gradient. The advantage of DVR is that it preserves the internal information within the image and requires minimal pre-processing. Difficulties in the technique include occlusion from non-target features in the volume as well as high computational demand.

Additionally, specifying the required transformations to fine-tune the algorithm may be a complex task with a steep learning curve.

Isosurface rendering is technically easier to achieve, but requires significantly more effort within the pre-operative workflow. Features of interest must be segmented from the medical volumes and then represented geometrically. Geometric representations predominantly involve surface meshes composed of a number of vertices in space that define triangles to cover the surface of the structure. While the intensity information is lost from the original image, this approach allows for accurate surface representation without a heavy computational load – ideal for platforms with limited computational capability.

1.3.4 **Augmented Reality in Medicine and Surgery**

Although AR has the potential to be a valuable tool for both surgeons as well as trainees, a surgical AR system must abide by a higher set of standards than other AR systems since errors in AR guidance can result in surgical errors or complications, which can cause significant damage to the patient. Therefore, tracking implementations used in surgical AR must be highly precise in order to prevent this from occurring. In addition, since human organs and tissue are not rigid, they typically do not behave as expected throughout the operation, and therefore the surgeon must take additional caution when using and relying on an AR system [64]. Another important consideration for surgical AR applications is the surgical workflow. For an AR system to be useful in a clinical context, it must be readily available and not provide a significant change in the existing workflow [69]. It is also vital that any image processing required to prepare the anatomical structures used in AR systems does not significantly impede the standard workflow [67]. It is important to note the variability of an AR system, and how the fundamental components, including definition of accuracy, image acquisition, registration,

software interfaces, localization and tracking devices, integration of real-time data, and most importantly, judgment and clinical experience, contribute to the variability and probability for error and must be carefully addressed when designing a surgical AR system [70].

Several groups have recently been working towards bringing augmented reality into the field of medicine and image-guided surgery. One particular group explored the application of AR to improve upon the traditional methods of viewing medical images, by developing an interactive display device that uses a Time-Of-Flight camera to provide AR tracking via surface matching algorithms [71]. By aiming the device at a patient, medical images were overlaid such that the user was able to interpret the images with additional spatial context relative to the patient. In work completed by Müller *et al.*, an augmented reality mobile device was evaluated for use with assisting clinicians with the insertion of needles for percutaneous nephrolithotomy. Results from this study indicated that trainees performed best with respect to needle insertion time while using the AR device, while experts performed best under traditional fluoroscopic guidance [72]. In work performed by Masutani *et al.*, an AR visualization system was developed to allow 3D vascular models to be overlaid on live X-ray fluoroscopy by using 2D to 3D registration via fiducial markers [73]. Another group used a see-through HMD device to implement AR that acted to overlay segmented 3D virtual objects onto the brain for the purpose of cranial neurosurgery. For this particular implementation, IR reflective markers were used to perform tracking of the subject, in this case a head phantom. Different visualization techniques were discussed, including the use of wireframe models to improve user depth perception of the virtual objects [74]. Other groups have used similar techniques in other areas of surgery, including laparoscopy [75-78], and percutaneous needle-based procedures including biopsy [79] and focal ablation [80]. It is clear that the field of surgical AR is quickly growing and

has an excellent potential to assist both trainee and experienced surgeons to perform tasks more efficiently.

1.4 **Human Performance: Theory, Application**

The objective evaluation of human performance is important for enabling researchers to quantify the ability of a user to perform motor control tasks while using a particular device. Since many, if not all, modern surgical procedures require a surgeon to perform a series of tasks using human motor control, the application of objective evaluation methods is essential in order to understand and identify the underlying characteristics of a device that enables a user to perform optimally. Although there have been many proposed methods of human performance evaluation, our work focuses on the application and various extension of the Fitts' Law methodology, which involves the use of a human performance model that enables the quantification of human pointing task performance. The following section discusses the Fitts' Law methodology and the various extensions that have been developed to allow for the evaluation of tasks of different nature. Several different applications of this particular model are discussed, with a focus on surgical task performance evaluation. In addition, other performance evaluation methods are discussed.

1.4.1 **Fitts' Law**

In 1954, researcher Paul Fitts demonstrated that human performance for simple motor control tasks could be modeled using a theory adapted from the information science field [81]. This model identifies a relationship between speed and accuracy that can be evaluated by subjecting a user to a series of targeting tasks, each with varying difficulty. In order to quantify task difficulty, Fitts proposed the following formulation for index of difficulty for a particular one-dimensional task:

$$ID = -\log_2 \left(\frac{W}{2D} \right) \quad (1)$$

where ID represents index of difficulty in units of bits/response, W represents the tolerance range of the target (target width) and D represents the distance or amplitude of the target from the user's starting position to the centre of the target [81]. This representation was derived in a manner analogous to Shannon's theorem (for the information capacity of a communication channel) by Fitts with the assumption that the logarithm of the signal-to-noise (SNR) ratio corresponds to the resolution of a signal into quanta that have bands of tolerance [81-83]. Many researchers have developed and applied different variations for the formulation of index of difficulty. Welford's variation has been adopted by many researchers as it often results in more optimal results.

$$ID = \log_2 \left(\frac{D}{W} + 0.5 \right) \quad (2)$$

By comparing this with Shannon's theorem, the SNR is equivalent to the ratio of target amplitude to target width in Fitts' original equation, and since Fitts' original experiments had D:W ratios as low as 1:1, it is noted that it may be more favorable to use the direct analogy to Shannon's theorem as follows:

$$ID = \log_2 \left(\frac{D}{W} + 1 \right) \quad (3)$$

This particular model ensures that task difficulty is always positive, which is a necessary condition, since a negative task difficulty would contradict the theory underlying the human performance models in question (i.e. what would a negative task difficulty imply?). It should be also noted, as [82] implies: there is no particular model that is "correct", since each formulation is only a representative of a human performance task, although there is still much debate over which model should be used [84]. What is important to

note is that these logarithmic expressions all provide relative measures which allow subsequent measures to be compared objectively.

Upon selecting the task difficulty model, it must be ensured that an adequate range of task difficulties are selected in order to fully evaluate a user's performance for a range of conditions. MacKenzie *et al.* suggest that a range of 2-8 bits shall be selected in each Fitts' Law related experiment, and that the user performs each task difficulty condition around 15-25 times so that a performance tendency can be observed [85]. During each task, the movement time of each task is recorded such that the following linear trade-off of speed and accuracy can be determined as follows:

$$MT = C_1 + C_2 \cdot ID \quad (4)$$

where MT represents observed movement time, ID represents index of difficulty as discussed above, and C_1 and C_2 represent experimentally determined parameters calculated by a linear regression of the collected data. It can be noted that by rearranging the linear equation in (4), the value of $1/C_2$ can be interpreted as the index of performance, or IP , measured in bits per second (bps).

To further improve the correlation between speed and accuracy, [82] suggest that adjustments for accuracy can be applied to the observed task completion times in order to fully represent a user's "actual" performance. By analyzing the collected end-point data, an effective target width, denoted We , can be determined as:

$$We = 4.133\sigma \quad (5)$$

where σ represents the standard deviation of measured end-point positions calculated independently for each user and for each condition. In addition, an effective distance De can be determined. Effective distance is determined by

calculating the mean movement distance between a user's starting and end-point position independently for each user under each condition. Using both adjusted values to calculate an accuracy adjusted index of difficulty as follows:

$$ID = \log_2 \left(\frac{De}{We} + 1 \right) \quad (6)$$

It should be additionally noted, that the above models for index of difficulty were originally developed for discrete translational tasks, however the model has been shown to provide similar results for rotational tasks, where instead of translational units of D and W , angular units can be substituted [86].

1.4.2 **Application**

The predictive abilities of the Fitts' Law methodology are often used in graphical user interface (GUI) design, where it is useful to predict the amount of time a user takes to perform a task, such as pointing and clicking on a button dialog. Soukoreff *et al.* used this model to examine and predict the performance of users instructed to spell out words using a stylus-based soft-keyboard [87]. In order to examine multiple tasks (each letter of the word), the Fitts' movement times were summed over each letter-to-letter movement of the stylus. Effectively, the larger task of spelling a word was broken down into smaller sub-tasks that were modeled using Fitts' Law [87]. Another example of the application of Fitts' Law for GUI development and optimization was presented by [88], where commonly used buttons and menus were either placed closer to the input device (i.e. computer mouse) or the targets themselves were enlarged to allow for increased user proficiency as a result of decreased index of difficulty and therefore task time. In work performed by Bi *et al.*, a variation of Fitts' law was used to model user performance for a set of touchscreen based interaction tasks [89]. Fitts' Law

has also been used to explore the interaction of users with an augmented reality mobile application for selecting buildings in an urban area, as shown by Rohs *et al.* [90]. In addition, Fitts' Law has been used in the field of laparoscopic surgery, cardiovascular surgery, as well as neurosurgery to assess the surgical skill of surgeons performing tasks with respect to varying magnification, task amplitude, and approach angle [91-94].

1.4.3 **Additional Performance Evaluation Methods**

Although Fitts' Law is capable of accurately describing the trade-off between speed and accuracy for human motor control tasks, other methods of evaluating human performance in surgery have been developed and applied in human performance evaluation research. For instance, there has been a great deal of interest in the objective evaluation of laparoscopic surgical skill since it is relatively new field of surgery and requires a high degree of skill compared to traditional open-abdominal surgery [95, 96]. This is due to reduced instrument maneuverability, impaired vision of the surgical field, and decreased tactile sensation [97]. In the past, techniques such as the Halstedian Technique had expert surgeons evaluate novice surgeons based on witnessed performance, however it has been noted that this method is prone to variation in how performance is rated due to subjectivity [98]. In contrast, objective evaluation techniques were introduced by Martin *et al.* that compared the difference in global ratings forms, operation-specific checklists and pass/fail judgments for the evaluation of surgeons working both on live animals, as well as simulators. This study determined that global ratings forms were capable of discriminating between levels of residents, while the checklists and pass/fail judgments were not [99]. Alternative methods were proposed through the development Imperial College Surgical Assessment Device, which uses video recording and motion analysis software to further assess performance in the following areas: compact spatial distribution of the instrument tip, smooth motion, depth perception, response

orientation, and ambidexterity [100]. Furthermore, techniques involving the application of algorithms such as Hidden Markov models have been applied to hand movements in laparoscopic surgery in order to compare the general behavior of a novice with an expert surgeon model [101, 102]. Although these findings indicate potentially viable methods for evaluating human performance, the Fitts' Law methodology remains as one of most widely used methods for evaluating motor task performance from the standpoint of speed and accuracy, which are arguably the two task metrics that form a basis for all motor control tasks. Since the following work focuses on the use and evaluation of novel devices for performing interventional tasks via discrete translational and rotational movements, we primarily utilized the Fitts' Law methodology for our evaluation.

References

1. R. Siegel, D. Naishadham and A. Jemal, "Cancer statistics, 2013," CA: Cancer J. Clin. **63**, 11-30 (2013).
2. Canadian Cancer Society's Advisory Committee on Cancer Statistics, "Canadian Cancer Statistics 2013", Toronto, ON: Canadian Cancer Society; 2013
3. B. B. Reeve, A. M. Stover, R. E. Jensen, R. C. Chen, K. L. Taylor, S. B. Clauser, S. P. Collins and A. L. Potosky, "Impact of diagnosis and treatment of clinically localized prostate cancer on health-related quality of life for older Americans," Cancer **118**, 5679-5687 (2012).
4. A. L. Potosky, J. Legler, P. C. Albertsen, J. L. Stanford, F. D. Gilliland, A. S. Hamilton, J. W. Eley, R. A. Stephenson and L. C. Harlan, "Health outcomes after prostatectomy or radiotherapy for prostate cancer: results from the Prostate Cancer Outcomes Study," Journal of the National Cancer Institute **92**, 1582-1592 (2000).
5. D. T. Eton and S. J. Lepore, "Prostate cancer and health-related quality of life: a review of the literature," Psycho-Oncology **11**, 307-326 (2002).
6. J. T. Wei, R. L. Dunn, H. M. Sandler, P. W. McLaughlin, J. E. Montie, M. S. Litwin, L. Nyquist and M. G. Sanda, "Comprehensive comparison of health-related quality of life after contemporary therapies for localized prostate cancer," Journal of Clinical Oncology **20**, 557-566 (2002).

7. T. A. Stamey, N. Yang, A. R. Hay, J. E. McNeal, F. S. Freiha and E. Redwine, "Prostate-specific antigen as a serum marker for adenocarcinoma of the prostate," *New England Journal of Medicine* **317**, 909-916 (1987).
8. A. R. Rao, H. G. Motiwala and O. Karim, "The discovery of prostate-specific antigen," *BJU international* **101**, 5-10 (2008).
9. J. I. Izawa, L. Klotz, D. R. Siemens, W. Kassouf, A. So, J. Jordan, M. Chetner and A. E. Iansavichene, "Prostate cancer screening: Canadian guidelines 2011," *Canadian Urological Association Journal* **5**, 235 (2011).
10. H. Hricak, P. L. Choyke, S. C. Eberhardt, S. A. Leibel and P. T. Scardino, "Imaging Prostate Cancer: A Multidisciplinary Perspective 1," *Radiology* **243**, 28-53 (2007).
11. S. Ghai and A. Toi, "Role of transrectal ultrasonography in prostate cancer," *Radiologic Clinics of North America* **50**, 1061-1073 (2012).
12. E. K. Outwater and J. L. Montilla-Soler, "Imaging of Prostate Carcinoma," *Cancer Control* **20**, 161-176 (2013).
13. R. Clements, "Ultrasonography of prostate cancer," *European radiology* **11**, 2119-2125 (2001).
14. A. P. Kirkham, M. Emberton and C. Allen, "How good is MRI at detecting and characterising cancer within the prostate?," *European urology* **50**, 1163-1175 (2006).
15. A. Villers, L. Lemaitre, J. Haffner and P. Puech, "Current status of MRI for the diagnosis, staging and prognosis of prostate cancer: implications for focal therapy and active surveillance," *Current opinion in urology* **19**, 274-282 (2009).
16. G. J. Kelloff, P. Choyke and D. S. Coffey, "Challenges in clinical prostate cancer: role of imaging," *AJR. American journal of roentgenology* **192**, 1455 (2009).
17. L. Dickinson, H. U. Ahmed, C. Allen, J. O. Barentsz, B. Carey, J. J. Futterer, S. W. Heijmink, P. J. Hoskin, A. Kirkham and A. R. Padhani, "Magnetic resonance imaging for the detection, localisation, and characterisation of prostate cancer: recommendations from a European consensus meeting," *European urology* **59**, 477-494 (2011).
18. Y. Mazaheri, A. Shukla-Dave, A. Muellner and H. Hricak, "MR imaging of the prostate in clinical practice," *Magnetic Resonance Materials in Physics, Biology and Medicine* **21**, 379-392 (2008).
19. M. B. Amin, *Gleason grading of prostate cancer: a contemporary approach*. (Lippincott Williams & Wilkins, 2004).

20. G. L. Andriole, "Pathology: the lottery of conventional prostate biopsy," *Nature Reviews Urology* **6**, 188-189 (2009).
21. C. R. King, J. E. McNeal, H. Gill and J. C. Presti Jr, "Extended prostate biopsy scheme improves reliability of Gleason grading: implications for radiotherapy patients," *International Journal of Radiation Oncology* Biology* Physics* **59**, 386-391 (2004).
22. U. Patel and D. Rickards, *Handbook of transrectal ultrasound and biopsy of the prostate*. (Informa Health Care, 2002).
23. C. M. Moore, N. L. Robertson, N. Arsanious, T. Middleton, A. Villers, L. Klotz, S. S. Taneja and M. Emberton, "Image-guided prostate biopsy using magnetic resonance imaging-derived targets: a systematic review," *European urology* **63**, 125-140 (2013).
24. J. Bax, D. Cool, L. Gardi, K. Knight, D. Smith, J. Montreuil, S. Sherebrin, C. Romagnoli and A. Fenster, "Mechanically assisted 3D ultrasound guided prostate biopsy system," *Medical physics* **35**, 5397-5410 (2008).
25. D. Keetch, W. Catalona and D. Smith, "Serial prostatic biopsies in men with persistently elevated serum prostate specific antigen values," *The Journal of urology* **151**, 1571-1574 (1994).
26. J. V. Hegde, R. V. Mulkern, L. P. Panych, F. M. Fennessy, A. Fedorov, S. E. Maier and C. Tempany, "Multiparametric MRI of prostate cancer: An update on state-of-the-art techniques and their performance in detecting and localizing prostate cancer," *Journal of Magnetic Resonance Imaging* **37**, 1035-1054 (2013).
27. J. Haffner, L. Lemaitre, P. Puech, G. P. Haber, X. Leroy, J. S. Jones and A. Villers, "Role of magnetic resonance imaging before initial biopsy: comparison of magnetic resonance imaging-targeted and systematic biopsy for significant prostate cancer detection," *BJU international* **108**, E171-E178 (2011).
28. B. K. Park, J. W. Park, S. Y. Park, C. K. Kim, H. M. Lee, S. S. Jeon, S. I. Seo, B. C. Jeong and H. Y. Choi, "Prospective evaluation of 3-T MRI performed before initial transrectal ultrasound-guided prostate biopsy in patients with high prostate-specific antigen and no previous biopsy," *American Journal of Roentgenology* **197**, W876-W881 (2011).
29. B. A. Hadaschik, T. H. Kuru, C. Tulea, P. Rieker, I. V. Popeneciu, T. Simpfendörfer, J. Huber, P. Zogal, D. Teber and S. Pahernik, "A novel stereotactic prostate biopsy system integrating pre-interventional magnetic resonance imaging and live ultrasound fusion," *The Journal of urology* **186**, 2214-2220 (2011).
30. G. A. Sonn, S. Natarajan, D. J. Margolis, M. MacAiran, P. Lieu, J. Huang, F. J. Dorey and L. S. Marks, "Targeted biopsy in the detection of prostate cancer using an

- office based magnetic resonance ultrasound fusion device," *The Journal of urology* **189**, 86-92 (2013).
31. J. A. Kusske, P. T. Turner, G. A. Ojemann and A. B. Harris, "Ventriculostomy for the treatment of acute hydrocephalus following subarachnoid hemorrhage," *Journal of neurosurgery* **38**, 591-595 (1973).
 32. S. A. Mayer and F. Rincon, "Treatment of intracerebral haemorrhage," *The Lancet Neurology* **4**, 662-672 (2005).
 33. P. Schödel, M. Proescholdt, O.-W. Ullrich, A. Brawanski and K.-M. Schebesch, "An outcome analysis of two different procedures of burr-hole trephine and external ventricular drainage in acute hydrocephalus," *Journal of Clinical Neuroscience* **19**, 267-270 (2012).
 34. P. Ferdinande, "Recommendations for intra-hospital transport of the severely head injured patient," *Intensive care medicine* **25**, 1441-1443 (1999).
 35. L. P. Voigt, S. M. Pastores, N. D. Raoof, H. T. Thaler and N. A. Halpern, "Review of a large clinical series: intrahospital transport of critically ill patients: outcomes, timing, and patterns," *Journal of intensive care medicine* **24**, 108-115 (2009).
 36. A. Saladino, J. B. White, E. F. Wijdicks and G. Lanzino, "Malplacement of ventricular catheters by neurosurgeons: a single institution experience," *Neurocritical care* **10**, 248-252 (2009).
 37. D. R. Huyette, B. J. Turnbow, C. Kaufman, D. F. Vaslow, B. B. Whiting and M. Y. Oh, "Accuracy of the freehand pass technique for ventriculostomy catheter placement: retrospective assessment using computed tomography scans," (2008).
 38. U. K. Kakarla, S. W. Chang, N. Theodore, R. F. Spetzler and L. J. Kim, "Safety and accuracy of bedside external ventricular drain placement," *Neurosurgery* **63**, ONS162-ONS167 (2008).
 39. C.-C. Hsia, Y.-H. CHen, H.-Y. Wu and M.-Y. Liu, "The misplacement of external ventricular drain by freehand method in emergent neurosurgery," *Acta Neurol. Belg* **111**, 22-28 (2011).
 40. R. T. Azuma, "A survey of augmented reality," *Presence* **6**, 355-385 (1997).
 41. F. Zhou, H. B.-L. Duh and M. Billinghurst, *Proceedings of the 7th IEEE/ACM International Symposium on Mixed and Augmented Reality*, 2008.
 42. M. Ribo, A. Pinz and A. L. Fuhrmann, *Instrumentation and Measurement Technology Conference, 2001. IMTC 2001. Proceedings of the 18th IEEE*, 2001.

43. A. Milne, D. Chess, J. Johnson and G. King, "Accuracy of an electromagnetic tracking device: a study of the optimal operating range and metal interference," *Journal of biomechanics* **29**, 791-793 (1996).
44. I. E. Sutherland, Proceedings of the December 9-11, 1968, fall joint computer conference, part I, 1968.
45. M. Pressigout and E. Marchand, Proceedings of the 5th IEEE and ACM International Symposium on Mixed and Augmented Reality, 2006.
46. H. Wuest, F. Vial and D. Strieker, Mixed and Augmented Reality, 2005. Proceedings. Fourth IEEE and ACM International Symposium on, 2005.
47. G. Bishop and S. Julier, "Tracking: how hard can it be?," *IEEE Computer Graphics and Applications* **22**, 0022-0023 (2002).
48. A. I. Comport, E. Marchand, M. Pressigout and F. Chaumette, "Real-time markerless tracking for augmented reality: the virtual visual servoing framework," *Visualization and Computer Graphics, IEEE Transactions on* **12**, 615-628 (2006).
49. K. W. Chia, A. D. Cheok and S. J. Prince, Mixed and Augmented Reality, 2002. ISMAR 2002. Proceedings. International Symposium on, 2002.
50. A. I. Comport, É. Marchand and F. Chaumette, Proceedings of the 2nd IEEE/ACM International Symposium on Mixed and Augmented Reality, 2003.
51. V. Ferrari, T. Tuytelaars and L. Van Gool, Augmented Reality, 2001. Proceedings. IEEE and ACM International Symposium on, 2001.
52. J. Park, S. You and U. Neumann, Proc. Int. Workshop on Augmented Reality, 1998.
53. L. Vacchetti, V. Lepetit and P. Fua, Mixed and Augmented Reality, 2004. ISMAR 2004. Third IEEE and ACM International Symposium on, 2004.
54. P. Lang, A. Kusej, A. Pinz and G. Bressier, Instrumentation and Measurement Technology Conference, 2002. IMTC/2002. Proceedings of the 19th IEEE, 2002.
55. A. Pinz, M. Brandner, H. Ganster, A. Kusej, P. Lang and M. Ribo, "Hybrid tracking for augmented reality," *ÖGAI Journal* **21**, 17-24 (2002).
56. T. Höllerer and S. Feiner, "Mobile augmented reality," *Telegeoinformatics: Location-Based Computing and Services*. Taylor and Francis Books Ltd., London, UK **21** (2004).
57. D. Van Krevelen and R. Poelman, "A survey of augmented reality technologies, applications and limitations," *International Journal of Virtual Reality* **9**, 1 (2010).

58. Y. Liu, X. Qin, S. Xu, E. Nakamae and Q. Peng, "Light source estimation of outdoor scenes for mixed reality," *The Visual Computer* **25**, 637-646 (2009).
59. F. A. Biocca and J. P. Rolland, "Virtual eyes can rearrange your body: Adaptation to visual displacement in see-through, head-mounted displays," *Presence: Teleoperators and Virtual Environments* **7**, 262-277 (1998).
60. S. R. Ellis, F. Breant, B. Manges, R. Jacoby and B. D. Adelstein, *Virtual Reality Annual International Symposium, 1997.*, IEEE 1997, 1997.
61. T. Sielhorst, M. Feuerstein and N. Navab, "Advanced medical displays: A literature review of augmented reality," *Display Technology, Journal of* **4**, 451-467 (2008).
62. R. R. Shamir, M. Horn, T. Blum, J.-H. Mehrkens, Y. Shoshan, L. Joskowicz and N. Navab, *Biomedical Imaging: From Nano to Macro, 2011 IEEE International Symposium on*, 2011.
63. K. Kiyokawa, M. Billinghamurst, B. Campbell and E. Woods, *Proceedings of the 2nd IEEE/ACM International Symposium on Mixed and Augmented Reality*, 2003.
64. J. H. Shuhaiber, "Augmented reality in surgery," *Archives of surgery* **139**, 170-174 (2004).
65. R. Raskar, J. Van Baar, P. Beardsley, T. Willwacher, S. Rao and C. Forlines, *ACM SIGGRAPH 2006 Courses*, 2006.
66. M. Hegarty, M. Keehner, C. Cohen, D. R. Montello and Y. Lippa, "The role of spatial cognition in medicine: Applications for selecting and training professionals," *Applied spatial cognition*, 285-315 (2007).
67. J. Traub, P. Stefan, S. M. Heining, T. Sielhorst, C. Riquarts, E. Euler and N. Navab, "Hybrid navigation interface for orthopedic and trauma surgery," in *Medical Image Computing and Computer-Assisted Intervention–MICCAI 2006*, (Springer, 2006), pp. 373-380.
68. Q. Zhang, T. M. Peters and R. Eagleson, "Medical Image Volumetric Visualization: Algorithms, Pipelines, and Surgical Applications," in *Medical Image Processing*, (Springer, 2011), pp. 291-317.
69. N. Navab, J. Traub, T. Sielhorst, M. Feuerstein and C. Bichlmeier, "Action-and workflow-driven augmented reality for computer-aided medical procedures," *Computer Graphics and Applications, IEEE* **27**, 10-14 (2007).
70. S.-L. Tang, C.-K. Kwok, M.-Y. Teo, N. W. Sing and K.-V. Ling, "Augmented reality systems for medical applications," *Engineering in Medicine and Biology Magazine, IEEE* **17**, 49-58 (1998).

71. L. Maier-Hein, A. M. Franz, M. Fangerau, M. Schmidt, A. Seitel, S. Mersmann, T. Kilgus, A. Groch, K. Yung and T. R. dos Santos, "Towards mobile augmented reality for on-patient visualization of medical images," in *Bildverarbeitung für die Medizin 2011*, (Springer, 2011), pp. 389-393.
72. M. Müller, M.-C. Rassweiler, J. Klein, A. Seitel, M. Gondan, M. Baumhauer, D. Teber, J. J. Rassweiler, H.-P. Meinzer and L. Maier-Hein, "Mobile augmented reality for computer-assisted percutaneous nephrolithotomy," *International journal of computer assisted radiology and surgery* **8**, 663-675 (2013).
73. Y. Masutani, T. Dohi, F. Yamane, H. Iseki and K. Takakura, "Augmented reality visualization system for intravascular neurosurgery," *Computer aided surgery* **3**, 239-247 (1998).
74. C. R. Maurer Jr, F. Sauer, B. Hu, B. Bascle, B. Geiger, F. Wenzel, F. Recchi, T. Rohlfing, C. R. Brown and R. J. Bakos, *Medical Imaging 2001*, 2001.
75. H. Fuchs, M. A. Livingston, R. Raskar, K. Keller, J. R. Crawford, P. Rademacher, S. H. Drake and A. A. Meyer, *Augmented reality visualization for laparoscopic surgery*. (Springer, 1998).
76. J. Marescaux, F. Rubino, M. Arenas, D. Mutter and L. Soler, "Augmented-reality–assisted laparoscopic adrenalectomy," *Jama* **292**, 2211-2215 (2004).
77. P. Lamata, W. Ali, A. Cano, J. Cornella, J. Declerck, O. J. Elle, A. Freudenthal, H. Furtado, D. Kalkofen and E. Naerum, "Augmented reality for minimally invasive surgery: overview and some recent advances," *Augmented Reality*, 73-98 (2010).
78. L.-M. Su, B. P. Vagvolgyi, R. Agarwal, C. E. Reiley, R. H. Taylor and G. D. Hager, "Augmented reality during robot-assisted laparoscopic partial nephrectomy: toward real-time 3D-CT to stereoscopic video registration," *Urology* **73**, 896-900 (2009).
79. F. K. Wacker, S. Vogt, A. Khamene, J. A. Jesberger, S. G. Nour, D. R. Elgort, F. Sauer, J. L. Duerk and J. S. Lewin, "An Augmented Reality System for MR Image–guided Needle Biopsy: Initial Results in a Swine Model 1," *Radiology* **238**, 497-504 (2006).
80. S. Nicolau, A. Garcia, X. Pennec, L. Soler and N. Ayache, "An augmented reality system to guide radio-frequency tumour ablation," *Computer animation and virtual worlds* **16**, 1-10 (2005).
81. P. M. Fitts, "The information capacity of the human motor system in controlling the amplitude of movement," *Journal of experimental psychology* **47**, 381 (1954).
82. I. S. MacKenzie, "Fitts' law as a research and design tool in human-computer interaction," *Human-computer interaction* **7**, 91-139 (1992).

83. I. S. MacKenzie, "A note on the information-theoretic basis for Fitts' law," *Journal of Motor Behavior* **21**, 323-330 (1989).
84. E. R. Hoffmann, "Which version/variation of Fitts' law? A critique of information-theory models," *Journal of motor behavior* **45**, 205-215 (2013).
85. R. W. Soukoreff and I. S. MacKenzie, "Towards a standard for pointing device evaluation, perspectives on 27 years of Fitts' law research in HCI," *International Journal of Human-Computer Studies* **61**, 751-789 (2004).
86. G. V. Kondraske, Engineering in Medicine and Biology Society, 1994. *Engineering Advances: New Opportunities for Biomedical Engineers*. Proceedings of the 16th Annual International Conference of the IEEE, 1994.
87. R. William Soukoreff and I. Scott Mackenzie, "Theoretical upper and lower bounds on typing speed using a stylus and a soft keyboard," *Behaviour & Information Technology* **14**, 370-379 (1995).
88. S. K. Card, T. P. Moran and A. Newell, "The keystroke-level model for user performance time with interactive systems," *Communications of the ACM* **23**, 396-410 (1980).
89. X. Bi, Y. Li and S. Zhai, Proceedings of the SIGCHI Conference on Human Factors in Computing Systems, 2013.
90. M. Rohs, A. Oulasvirta and T. Suomalainen, Proceedings of the SIGCHI Conference on Human Factors in Computing Systems, 2011.
91. C. J. Lin and H.-J. Chen, "The Investigation of Laparoscopic Instrument Movement Control and Learning Effect," *BioMed Research International* **2013**, 16 (2013).
92. K. Abhari, J. S. Baxter, E. S. Chen, A. R. Khan, C. Wedlake, T. Peters, R. Eagleson and S. de Ribaupierre, "The role of augmented reality in training the planning of brain tumor resection," in *Augmented Reality Environments for Medical Imaging and Computer-Assisted Interventions*, (Springer, 2013), pp. 241-248.
93. C. A. Linte, J. White, R. Eagleson, G. M. Guiraudon and T. M. Peters, "Virtual and augmented medical imaging environments: Enabling technology for minimally invasive cardiac interventional guidance," *Biomedical Engineering, IEEE Reviews in* **3**, 25-47 (2010).
94. K. Abhari, J. H. Baxter, E. Chen, A. Khan, C. Wedlake, T. Peters, S. de Ribaupierre and R. Eagleson, "Use of a Mixed-Reality System to Improve the Planning of Brain Tumour Resections: Preliminary Results," in *Augmented Environments for Computer-Assisted Interventions, Vol. 7815*, edited by C. Linte, E. S. Chen, M.-O. Berger, J. Moore and D. Holmes, III (Springer Berlin Heidelberg, 2013), pp. 55-66.

95. A. Karniel and G. F. Inbar, "A model for learning human reaching movements," *Biological cybernetics* **77**, 173-183 (1997).
96. A. Gallagher, N. McClure, J. McGuigan, I. Crothers and J. Browning, "Virtual reality training in laparoscopic surgery: a preliminary assessment of minimally invasive surgical trainer virtual reality (MIST VR)," *Endoscopy* **31**, 310-313 (1999).
97. M. T. Gettman, G. V. Kondraske, O. Traxer, K. Ogan, C. Napper, D. B. Jones, M. S. Pearle and J. A. Cadeddu, "Assessment of basic human performance resources predicts operative performance of laparoscopic surgery," *Journal of the American College of Surgeons* **197**, 489-496 (2003).
98. R. W. Barnes, N. P. Lang and M. F. Whiteside, "Halstedian technique revisited. Innovations in teaching surgical skills," *Annals of surgery* **210**, 118 (1989).
99. J. Martin, G. Regehr, R. Reznick, H. MacRae, J. Murnaghan, C. Hutchison and M. Brown, "Objective structured assessment of technical skill (OSATS) for surgical residents," *British Journal of Surgery* **84**, 273-278 (1997).
100. N. Stylopoulos and K. G. Vosburgh, "Assessing technical skill in surgery and endoscopy: a set of metrics and an algorithm (C-PASS) to assess skills in surgical and endoscopic procedures," *Surgical innovation* **14**, 113-121 (2007).
101. L. Rabiner, "A tutorial on hidden Markov models and selected applications in speech recognition," *Proceedings of the IEEE* **77**, 257-286 (1989).
102. G. Megali, S. Sinigaglia, O. Tonet and P. Dario, "Modelling and evaluation of surgical performance using hidden Markov models," *Biomedical Engineering, IEEE Transactions on* **53**, 1911-1919 (2006).

Chapter 2

2. Evaluating Human Performance for Needle Guidance Tasks Using a Prostate Biopsy Device[†]

2.1 Introduction

Prostate cancer is among the leading causes of death in men in North America, with an estimated 238,590 new cases in the United States in 2013 [1]. In many instances, early diagnosis of this disease can allow for effective treatment and management of the disease [2]. A number of techniques exist to diagnose prostate cancer including prostate specific antigen (PSA) test, digital rectal exam (DRE), prostate biopsy, and imaging. A biopsy of the prostate is often performed under transrectal ultrasound (TRUS) guidance, and allows a clinician to guide a specialized needle into the prostate (see Figure 2-1) to collect samples of prostate tissue (biopsy cores) for analysis by a pathologist to detect the presence and grade of cancer at each of the biopsied regions. In a typical biopsy procedure, an average of 10 biopsy cores are acquired from the patient's prostate [3]. This method is prone to generating a false-negative result upon the patient's initial biopsy procedure, leading to mischaracterization of the disease and requiring the patient to undergo additional repeat biopsy procedures [4]. Recently, a device was developed by [5] to provide navigation for performing targeted prostate biopsy based on imaging to ensure that physicians could collect tissue samples at precise 3D positions within the prostate. Using a tracked passive mechanical arm along with a 3D ultrasound (US) imaging system, the device enables biopsy core centre targeting accuracy of approximately 3.87 ± 1.81 mm [5].

[†]. A version of this chapter is being prepared for submission to IEEE Transactions on Systems, Man, and Cybernetics: Kramers, M., Fenster, A., Eagleson, R.

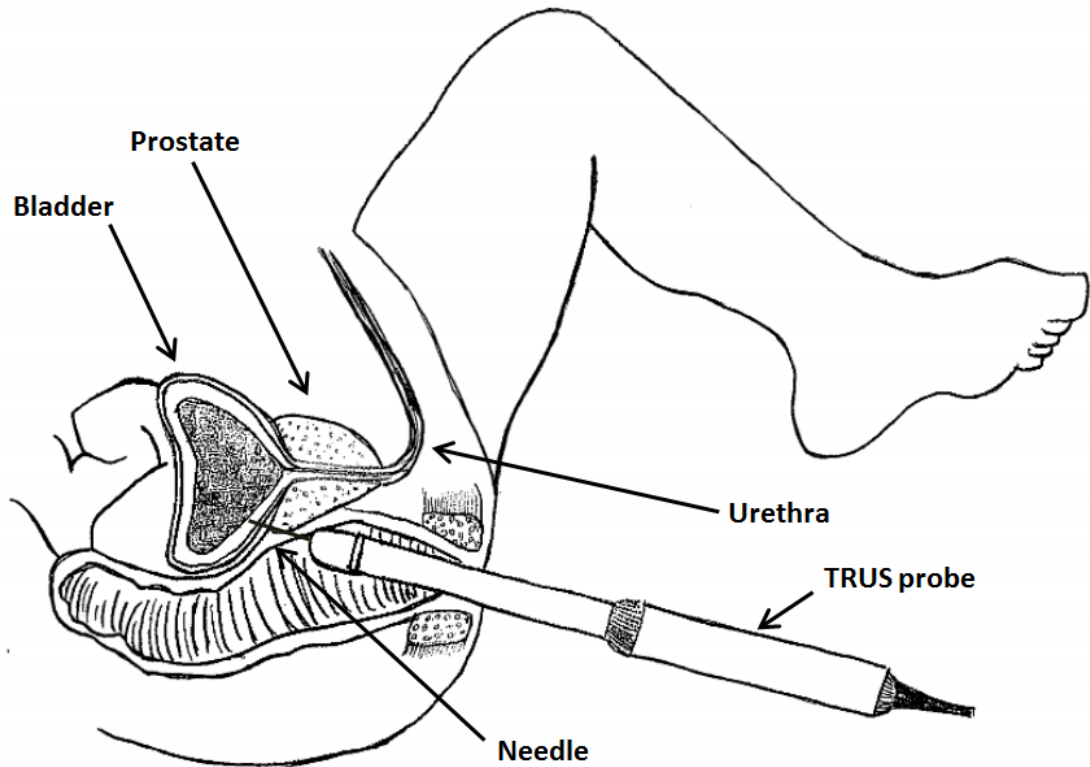


Figure 2-1: Biopsy procedure schematic with TRUS probe inserted into the patient's rectum along with needle aligned in parallel to the ultrasound image plane

With the amount of prostate cancer related deaths reaching an estimated total of 29,720 in the United States in 2013 [1], it becomes increasingly necessary to make the biopsy procedure as efficient as possible so that the maximum number of patients can be diagnosed and treated effectively. A study performed by [6] demonstrates the increased accuracy of simulated biopsies performed using guided 3D guidance compared to 2D and 3D non-guided biopsies. Additionally, it was found that it took experts less time to perform guided 3D biopsies versus novices. The authors in this study however performed analysis on both time and accuracy as independent results. In order to determine the efficacy of a biopsy procedure with respect to both total biopsy core acquisition time and biopsy needle placement

accuracy, a unifying evaluation of performance must be established for objective evaluation of both the user and the device.

We propose a method for the objective evaluation of human performance for user's performing targeting tasks with the prostate biopsy device. Although there have been a number of groups focusing on evaluation of human performance in laparoscopic surgery [7-9], there has been limited focus on the objective evaluation of human performance for needle guidance tasks. It is therefore important to apply and validate a standardized method for evaluating human performance for such procedures.

2.2 Modeling Image-Guided Human Performance

We base our evaluation on the Fitts' Law human movement model [10], which models the relationship between speed and accuracy for human pointing tasks. Fitts' Law has been used in an assortment of graphical user interface evaluation and optimization studies [11, 12], as it allows designers to evaluate how well users are able to perform pointing tasks within a graphically driven environment. The basis of this paradigm is that a target can be parameterized by its size as well as its distance from a user's starting position. Using these values, an index of difficulty for a given targeting task can be calculated using the following Shannon formulation [13]:

$$ID = \log_2 \left(\frac{D}{W} + 1 \right) \quad (1)$$

where ID denotes index of difficulty, D denotes translational distance between user starting position and target centre, and W denotes target width. The index of difficulty is then used in the following linear equation to relate to task completion time:

$$MT = C_1 + C_2 \cdot ID \quad (2)$$

where MT denotes task movement time, and C_1 and C_2 denote experimentally determined constants. C_2 can be interpreted as the slope of the linear regression formed by this relationship, and $1/C_2$ can be interpreted as the index of performance, or IP , measured in bits per second (bps).

By subjecting users to targets with a range of index of difficulties and measuring the associated movement time for each task, a speed-accuracy trade-off can be observed by performing a linear regression against MT and ID , and an index of performance can be determined for a particular user. It should be noted, that since the index of difficulty of each task is composed of a ratio of two parameters, rotational tasks can be considered in the same way as translational tasks by using units of degrees instead of translational distance measurements [14, 15].

In addition to the traditional formulation of index of performance, [16] suggest that adjustments for accuracy should be applied to the collected data in order to represent a user's actual performance. By using the collected end-point data, an effective target width, denoted We , can be determined as

$$We = 4.133\sigma \quad (3)$$

where σ represents the standard deviation of measured end-point positions for each user for each condition. To further account for accuracy, an effective distance De can be calculated. Effective distance is determined by calculating the mean movement distance between the user's starting position and end-point position for each user under each condition. Using both adjusted values to calculate an accuracy adjusted index of difficulty as follows:

$$ID = \log_2 \left(\frac{De}{We} + 1 \right) \quad (4)$$

2.3 Methods

2.3.1 Prostate Biopsy Device

The prostate biopsy device consists of a tracked mechanical arm that affixes the TRUS probe and biopsy needle assembly (Figure 2-2). The mechanical arm was designed using a spherical linkage to create a remote centre of motion (RCM). As with many interventional procedures, the RCM is necessary for minimize patient damage from maneuvering tools within a single, confined entry point; in this case, the patient's rectum. Using encoders at each of the rotational axes of the linkage, along with a linear encoder aligned with the long axis of the TRUS probe, the position and orientation of the probe and needle can be computed with respect to the RCM. The device allows the TRUS probe and biopsy needle to be actuated by the user in 4 degrees of freedom (DOF), including three degrees of rotational freedom about the RCM. In addition, the probe and needle can be translated linearly in the axial direction to allow for insertion of the probe into the patient, as well as for any adjustments required to accommodate prostate movement during the procedure. For this study, we have excluded evaluation of the linear degree of freedom, since it ideally held fixed during the duration of the biopsy. We have also neglected the axial rotation degree of freedom since it was determined that each of the targets, when distributed on the surface of a sphere, could be acquired without having to rotate the probe axially. In the clinical setting, the device uses axial rotation of the TRUS probe to acquire and reconstruct the 3D prostate image, which is then registered to a pre-operative image containing the predetermined targeted regions. For this study, we excluded this image acquisition task, as it is only performed once at the beginning of the procedure and employs automatic segmentation algorithms which have a fixed processing time.

We have developed software to collect user movement data by computing the forward kinematics of the needle using the encoders. The visual interface

component of the software allows the user to visualize the relative position of the biopsy needle trajectory projection as a cursor and a target volume as shown in Figure 2-2. In this study, spherical targets were used to simulate target biopsy regions and were displayed in red. The graphical user interface updates the position of the biopsy needle at approximately 60 Hz, which provides minimal lag and sufficient visual feedback for the targeting tasks. To aid in the visualization of small targets, crosshairs were added to both the cursor as well as the displayed target so that users could identify the location of both objects quickly. To allow all chosen target configurations to be visualized on the monitor without modification of the magnification during the pointing tasks, the magnification of the visualization was selected to be of the same scale at the physical device. It should be noted that since the linear degree of freedom in the axial direction was held constant for this study, movement along this axis would result in a change in the visual scale of the interface visualization and would add an additional degree of difficulty to the tasks.

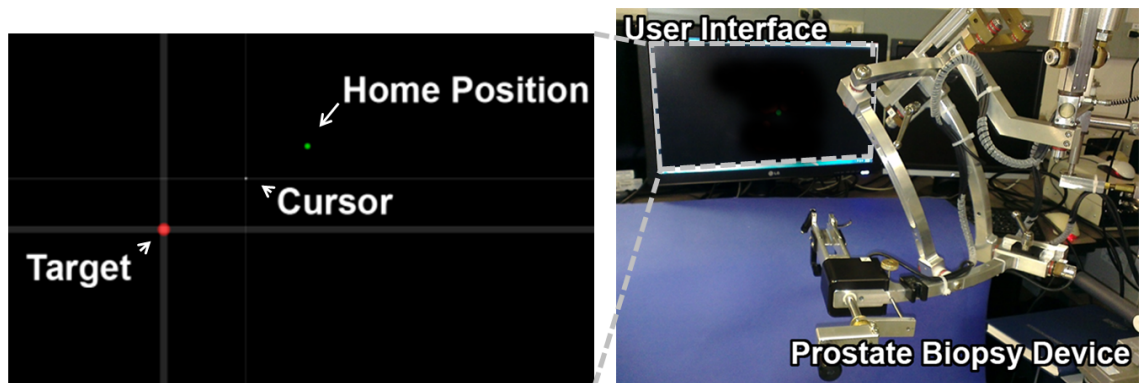


Figure 2-2: User Interface for visualization of biopsy needle and targets and Prostate Biopsy Device for performing targeting tasks

2.3.2 Targeting Task Design

To measure performance of users with the prostate biopsy device, we have created a set of 9 unique targets with varying difficulties shown in Table 2-1

which were performed at 12 equally spaced approach angles, resulting in a total of 108 unique target configurations. For each user, the order of the unique target configurations was randomized such that each user performed the tasks in a different order. In addition, each of the 108 target sets were repeated by each user a total of 3 times, with the sequence of each target configuration randomized between sets. To avoid any fatigue induced effect on performance, users were given 5 minute breaks between sets, and were also able to take breaks between targets when necessary.

Table 2-1: Target Distance and Tolerance Configuration Parameters

Condition	Target Distance (degrees)	Target Tolerance (degrees)	ID* (bits)
1	6	4	1.32
2	6	1	2.81
3	24	4	2.81
4	12	1	3.70
5	24	2	3.70
6	12	0.5	4.64
7	48	2	4.64
8	48	1	5.61
9	48	0.5	6.60

*Note that the Shannon formulation was used to calculate Index of Difficulty for each task configuration

According to [17], it is suggested methodological approach that the performance be estimated over a range of task difficulty between 2.0-8.0 bits in order to adequately quantify the normal range of human performance. It should be considered that in the clinical context of prostate biopsies, suspected tumor regions typically have a minimum size of 5 mm in diameter, so using this range of task difficulties will adequately take all biopsy target sizes into consideration. This was justified by the linear axial distance of the probe from the RCM was approximately 50 mm and the smallest target width of 0.5 degrees, and so using $50 \cdot \tan(0.5^\circ) \cong 0.44 \text{ mm}$ plus the inherent device error, determined that our method covered well beyond the smallest desirable

target width. It should be noted that tasks with difficulty above 6.6 bits were not practical to measure, since the targets would either exceed the full range of devices motion, would be too small for users to point to, or would not be practical with respect to the clinical biopsy procedure. Since the devices is actuated by rotation about a RCM, both target parameters are expressed in units of degrees, and therefore all of the targets are located on the surface of a sphere as shown in Figure 2-3. The users' view is directly along the z-axis in the 3D coordinate space, and therefore the users are able to visualize the targets as if they were projected onto a 2D plane (XY plane) as shown in Figure 2-3.

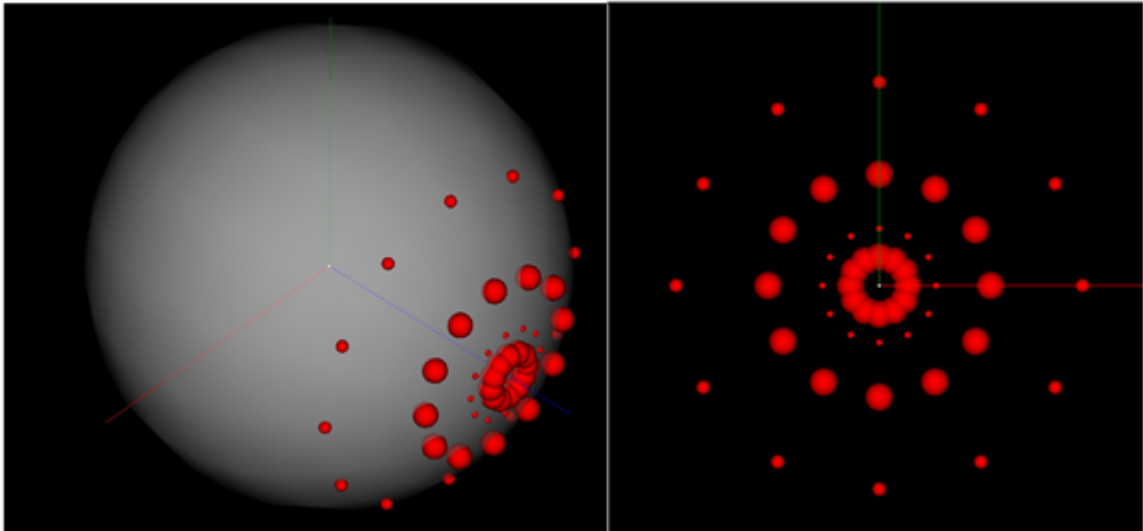


Figure 2-3: Isometric view of all target configurations and approach angles distributed on a sphere (left) and from users' viewpoint along the z-axis

2.3.3 Participants and Experimental Procedure

A total of 8 users, consisting of 7 males and 1 female with a mean age of 27.2 years (24-51 years), were selected at random from the Western University population to perform the targeting tasks using the device. One of the users had significant experience with operating the device in a laboratory setting. Each user was required to have experience with graphical user interfaces as

well as a practice session with the device to ensure that the targeting task procedure was fully understood. In the experiment, each user was required to place the projected biopsy needle cursor at a home position located at the centre of the RCM sphere. After pressing a footswitch connected to the device, one of 108 target configurations appeared on the display. The user was then required to move the cursor within the target by rotating the device about the RCM. Once the user was satisfied with the position of the cursor with respect to the target, the footswitch was again pressed to represent a biopsy core acquisition. The user was then instructed to return the cursor to the home position and press the footswitch again in order to initiate the next targeting task. This process was repeated for all 108 unique target configurations a total of 2 times. To reduce the effects of muscle memory on the users' performance, the target configuration order was randomized for each user for each iteration. During this process, the software recorded the target configuration parameters (target distance, width, and approach angle), the elapsed pointing time in milliseconds, as well as the complete trajectory of the cursor for each task at approximately 10 millisecond intervals throughout the experiment. Users were able to take a short break at intervals of 60 targets if they desired one.

2.3.4 Hypothesis

The focus of this experiment was to apply and validate a model to represent human performance for needle guidance tasks. The experiment described was tested against the following hypotheses (H):

H1. User performance with the prostate biopsy device conforms to the Fitts' Law model of human performance, indicating that there is a significant linear relationship between task difficulty and task completion time.

H2. The target approach angle does not contribute to users' performance as a result of device being unbalanced or difficult to maneuver. H3. An experienced user will have a higher index of performance compared to novice users.

2.4 Results

Upon collecting all of the movement data for all users, the results were analyzed to test whether Fitts' Law was indeed an appropriate model for explaining the performance of the users (H1). A one-way ANOVA test comparing each of the users' task completion time with the index of difficulty revealed that there was a significant relationship between task condition and completion time for all users ($F(9, 2307) = 213.09; p < 0.0001$ (9 task conditions, 2307 observed movement times). To test the second hypothesis (H2), an ANOVA test was used to compare the effect of approach angle on task completion time. There was found to be no significant contribution of approach angle on time and therefore our second hypothesis can be accepted, indicating that approach angle had no contribution to movement time. The final hypothesis was tested using an independent variable t-test. It was found that the experienced user had a significantly higher index of performance ($p < 0.05$) compared to the group of novice users, and therefore the third hypothesis (H3) can be accepted.

A Fitts' Law relationship for a single user is shown below in Figure 2-4.

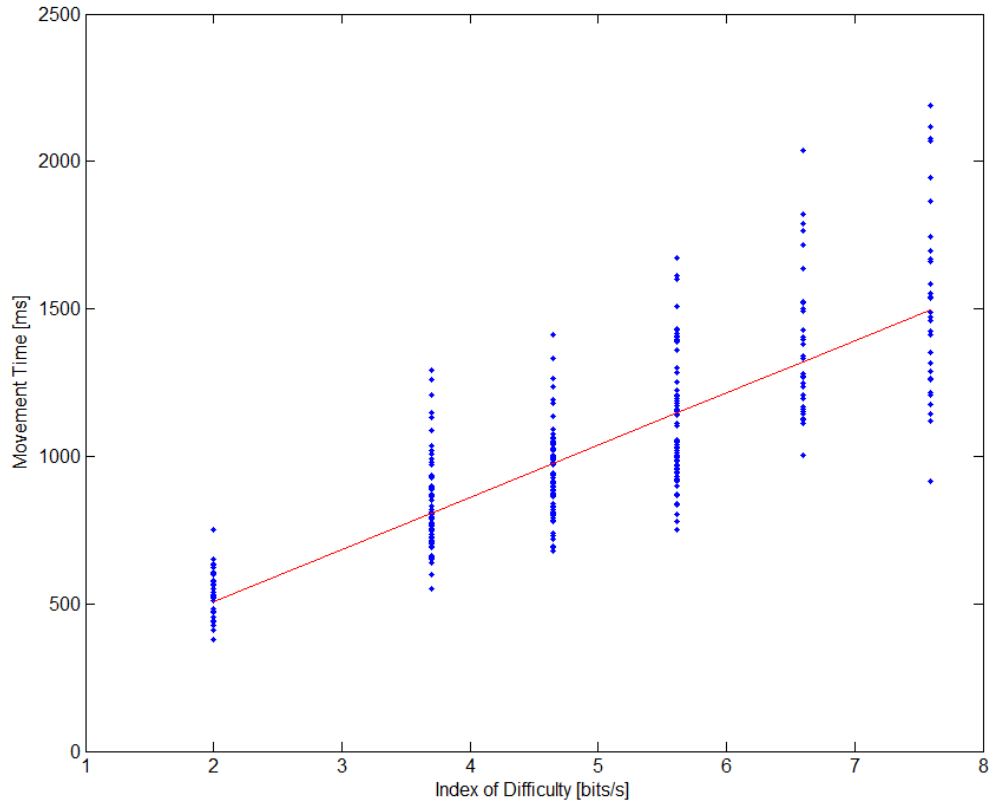


Figure 2-4: Fitts' Law profile and regression line for a single user for a total of 216 task configurations

All results were collected and linear regressions were performed on each users' index of difficulty versus movement time relationship. Using (2) and finding the inverse of C_2 , the index of performance was calculated along with the intercept. In addition, linear polynomial fitting was used to calculate the coefficient of determination (R^2) for each user. The results are displayed below in Table 2-2.

Table 2-2: Performance results for all users without adjustments to accuracy

User	Experience	Index of Performance [bits/s]	Intercept [ms]	R^2	Average Hit Rate [%]	F-Statistics (p<0.0001)
1	Expert	5.65	307.88	0.68	86.58	
2	Novice	4.88	201.67	0.51	92.06	$F(9, 2307)$ = 213.09
3	Novice	3.77	-131.28	0.63	98.09	
4	Novice	3.40	431.17	0.53	96.76	

5	Novice	4.15	766.53	0.46	89.61
6	Novice	4.16	136.58	0.63	89.02
7	Novice	4.08	177.08	0.57	89.37
8	Novice	3.37	407.24	0.46	95.10

As discussed in [16, 17], an adjustment for accuracy can be made to better account for users' actual performance during each pointing task experiment. The results after making the adjustments for accuracy are shown below in Table 2-3. It should be noted that the first degree of freedom in the ANOVA test for significance between task difficulty and movement time changed to represent the increased number of unique index of difficulties generated by the accuracy adjustment method.

Table 2-3: Performance results for all users with accuracy adjustments applied

User	Experience	Index of Performance [bits/s]	Intercept [ms]	R ²	F-Statistics (p<0.0001)
1	Expert	4.66	249.46	0.63	$F(71, 2307) = 56.80$
2	Novice	4.15	227.40	0.48	
3	Novice	3.63	-40.13	0.57	
4	Novice	3.22	446.39	0.41	
5	Novice	4.15	1027.8	0.37	
6	Novice	3.54	136.73	0.64	
7	Novice	3.47	152.17	0.48	
8	Novice	3.05	418.58	0.37	

In addition to the performance analysis using the Fitts' Law approach, the movement velocity profiles for each pointing task were observed. Figure 2-5 shows the averaged and normalized velocity profiles for each task condition. Velocity in each case was determined by calculating the tangential velocity, or the velocity in the direction of the target. This particular comparison is based strictly on the shape of the velocity profile; therefore each profile was normalized such that each trajectory was aligned at peak velocity.

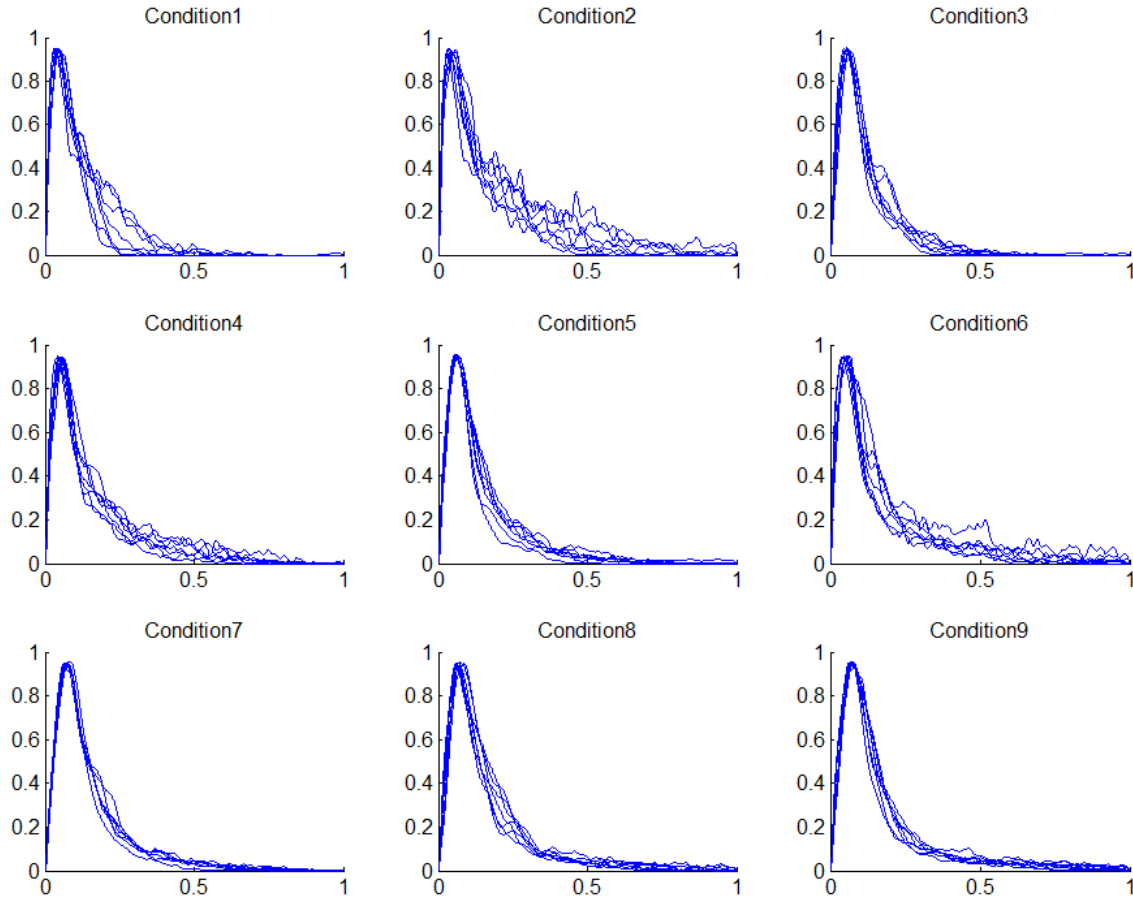


Figure 2-5: Tangential velocity profiles for all users averaged and normalized for each target condition.

2.5 Discussion

As demonstrated, Fitts' Methodology was adapted within this clinical context and Fitts' Law was used to provide an objective model of human performance for pointing tasks when using the prostate biopsy device. Prior to applying accuracy adjustments, the results for each user were comparable with the performance evaluation of other pointing devices, such as a stylus or computer mouse [17]. The fact that there was no significant relationship between approach angle and performance indicates that the prostate biopsy device is mechanically balanced such that users are able to actuate the TRUS probe in any direction with negligible degradation to performance. It is also

promising that the most experienced user of the device also attained the highest index of performance, indicating that additional training and time with the device can lead to higher performance, and this learning curve can be established using this methodology.

When accuracy adjustments were made, each index of performance, intercept, and coefficient of correlation typically decreased for the majority of users, although there was still a significant relationship between effective index of performance and movement time. Upon analysis it was found that the effective width had a larger impact than the effective distance when calculating the effective index of difficulty. This could indicate that there was a greater spread of end-point positions for each user, which may be a result of the mechanical arm momentum during actuation and resulting in larger over/under shooting of the target. Despite these discrepancies, the target hit rate was moderately high indicating that users were able to compensate for this additional momentum in most cases.

The tangential velocity profiles when visually compared show that there are trends among each individual condition. It appears that for conditions 1, 2, 4, and 6 there was much more variance on the deceleration phase of the velocity profile. To further investigate trends in the tangential velocity, the profiles were grouped by target distance (parameter A). By calculating the variance of each profile under each distance condition and then summing the variance along the time axis, the variance can be quantified and compared. As shown in Figure 2-6 and Table 2-4 below, the total variance decreases with increasing A . In other words, users had a tendency to follow a similar velocity trajectory pattern for longer target reaches.

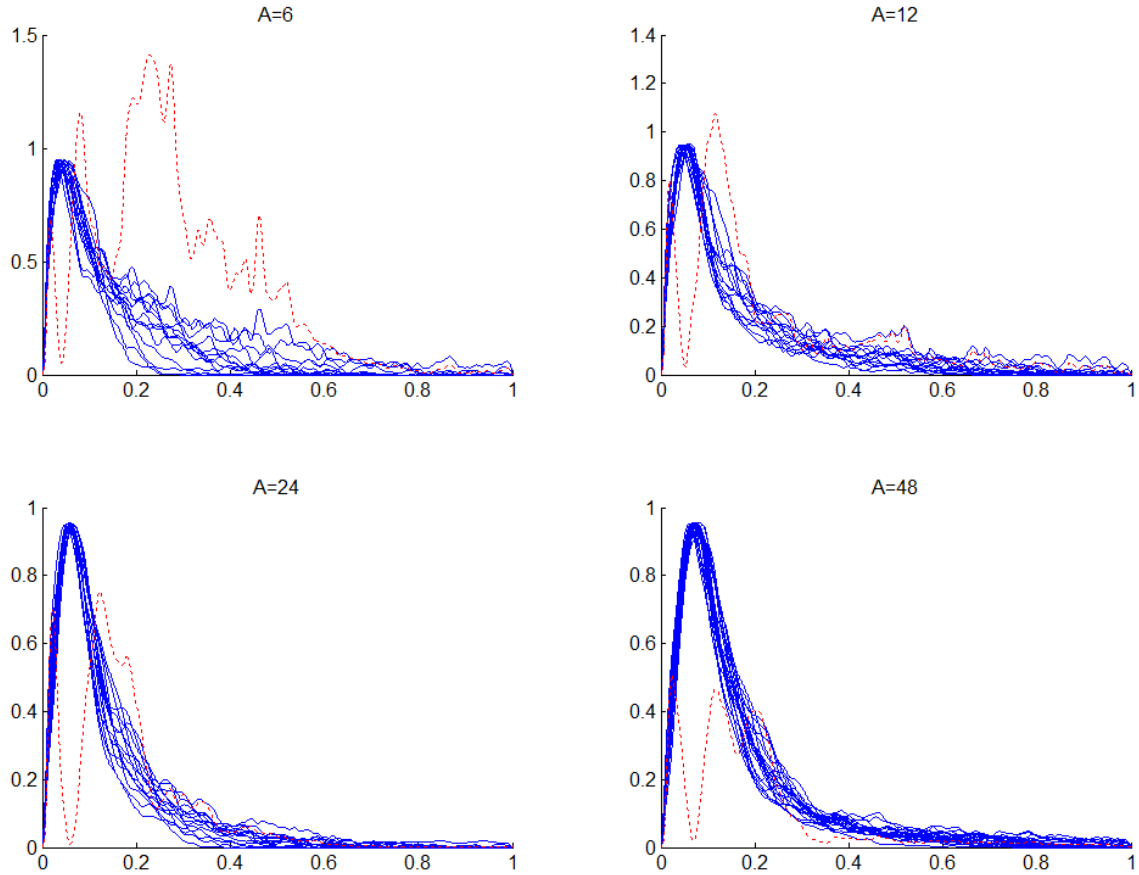


Figure 2-6: Tangential velocity profiles sorted by target distance (solid) and variance of each trajectory for all users (dotted)

Table 2-4: Sum of variance vs. target distance

Distance (A) (degrees)	Sum of Variance
6	19.494
12	9.2546
24	6.2015
48	4.5979

2.6 Conclusion

The work presented intended to provide a detailed methodology for the objective evaluation and quantification of human performance for users performing virtual needle guidance tasks on a prostate biopsy device. We have described the details of the application of Fitts' Methodology to prostate biopsy tasks and how the paradigm can be used to effectively evaluate users

and distinguish those with more experience with the device. This information is a crucial step towards optimization of both the prostate biopsy device as well as the procedural workflow.

References

1. R. Siegel, D. Naishadham and A. Jemal, "Cancer statistics, 2013," *CA: Cancer J. Clin.* **63**, 11-30 (2013).
2. J. A. Eastham and P. T. Scardino, "Early diagnosis and treatment of prostate cancer," *Disease-a-Month* **47**, 417-459 (2001).
3. G. L. Andriole, "Pathology: the lottery of conventional prostate biopsy," *Nature Reviews Urology* **6**, 188-189 (2009).
4. L. A. Eskew, R. L. Bare and D. L. McCullough, "Systematic 5 region prostate biopsy is superior to sextant method for diagnosing carcinoma of the prostate," *The Journal of urology* **157**, 199-203 (1997).
5. J. Bax, D. Cool, L. Gardi, K. Knight, D. Smith, J. Montreuil, S. Sherebrin, C. Romagnoli and A. Fenster, "Mechanically assisted 3D ultrasound guided prostate biopsy system," *Medical physics* **35**, 5397-5410 (2008).
6. D. W. Cool, M. J. Connolly, S. Sherebrin, R. Eagleson, J. I. Izawa, J. Amann, C. Romagnoli, W. M. Romano and A. Fenster, "Repeat Prostate Biopsy Accuracy: Simulator-based Comparison of Two-and Three-dimensional Transrectal US Modalities 1," *Radiology* **254**, 587-594 (2010).
7. C. J. Lin and H.-J. Chen, "The Investigation of Laparoscopic Instrument Movement Control and Learning Effect," *BioMed Research International* **2013**, 16 (2013).
8. D. B. Kaber, Y. Li, M. Clamann and Y.-S. Lee, "Investigating Human Performance in a Virtual Reality Haptic Simulator as Influenced by Fidelity and System Latency," *Systems, Man and Cybernetics, Part A: Systems and Humans, IEEE Transactions on* **42**, 1562-1566 (2012).
9. C. J. Lin, H.-J. Chen and Y.-C. Lo, "Ergonomic investigation of weight distribution of laparoscopic instruments," *Journal of Laparoendoscopic & Advanced Surgical Techniques* **21**, 411-415 (2011).
10. P. M. Fitts, "The information capacity of the human motor system in controlling the amplitude of movement," *Journal of experimental psychology* **47**, 381 (1954).
11. S. K. Card, T. P. Moran and A. Newell, "The keystroke-level model for user performance time with interactive systems," *Communications of the ACM* **23**, 396-410 (1980).

12. R. William Soukoreff and I. Scott Mackenzie, "Theoretical upper and lower bounds on typing speed using a stylus and a soft keyboard," Behaviour & Information Technology **14**, 370-379 (1995).
13. C. E. Shannon, "A mathematical theory of communication," ACM SIGMOBILE Mobile Computing and Communications Review **5**, 3-55 (2001).
14. A. Knight and P. Dagnall, "Precision in movements," Ergonomics **10**, 321-330 (1967).
15. G. V. Kondraske, Engineering in Medicine and Biology Society, 1994. Engineering Advances: New Opportunities for Biomedical Engineers. Proceedings of the 16th Annual International Conference of the IEEE, 1994.
16. I. S. MacKenzie, "Fitts' law as a research and design tool in human-computer interaction," Human-computer interaction **7**, 91-139 (1992).
17. R. W. Soukoreff and I. S. MacKenzie, "Towards a standard for pointing device evaluation, perspectives on 27 years of Fitts' law research in HCI," International Journal of Human-Computer Studies **61**, 751-789 (2004).

Chapter 3

3. A Mobile Augmented Reality Application for Image Guidance of Neurosurgical Interventions[†]

3.1 Related Work

According to the literature, tracking of an object's position is the main aspect which influences accuracy of a system and determines the level of interference with the medical workflow. The majority of AR systems take advantage of Head Mounted Displays (HMD), hand-held or fixed displays to show computer generated scenes to the user. Visualization techniques are used to incorporate preoperative medical images during the intervention as 3D objects rendered in real-time. Considering these three methods of AR, we can classify some recent work and indicate their advantages and deficiencies.

As an early prototype, in 1968 Sutherland et al. [1] developed a mechanical tracking system for their HMD 3D display. It was realized by attaching a mechanical linkage to the HMD which measured head position by computing axial displacement of the joints of a passive robotic arm. In similar work in 1992, Bajura *et al.* [2] replaced the mechanical linkage with electromagnetic sensors to determine the pose of a HMD and an ultrasound probe. Measuring position remotely (by magnetic or optical tracking systems) leads to a significant improvement in terms usability of the system, since they give more freedom to move the HMD within the operation site. Shamir et al. [3] used magnetic trackers and point based registration to align images, risk surfaces and segmented models to physical head models. In further work, Shamir et al. utilized the ability to track multiple objects simultaneously

[†]. A version of this paper has been published. Kramers, M., Armstrong, R., Bakhshmand, S.M., Fenster, A., de Ribaupierre, S., Eagleson, R., A Mobile Augmented Reality Application for Image Guidance of Neurosurgical Interventions. American Journal of Biomedical Engineering 2013, 3(6): 169-174

using optical tracking to develop an AR probe that incorporated a camera attached to a reference plate [4]. The output of the system was an augmented video image of the therapeutic site with relevant superimposed graphical content rendered according to the position of the probe. HMDs interfere with medical work flow and may restrict a surgeon's natural movement. As a result, hand held displays and cameras (AR probe as an example) are becoming more feasible within the operating room. DEX-ray [5] is a miniaturized version of a hand held probe with an integrated video camera. Naturally, in [4] and [5], displays are fixed at some point in operation room and a surgeon is required to switch between the real scene and the displayed AR scene, and thus increases the system's complexity. Mischkowski et al. found that camera and display units could be combined, as demonstrated by their X-scope [6]. X-Scope could be used for detection of bony segments in real-time and results were displayed on a hand held LCD. This configuration resembles current mobile devices. Infrared optical tracking became feasible by attaching reflective frames to portable display devices. These mobile devices enable surgeons to inspect patients from different points of view. In contrast, optical trackers impose limitations on this procedure, due to their limited workspace, necessity of attaching multiple reflectors to objects of interest and line of sight issues. An alternative method for tracking utilizes image-based tracking algorithms, which require adequate speed and accuracy. Fisher et al. developed a hybrid tracking scheme to calculate final estimation of the pose in an AR framework for a neurosurgical application [7]. Two streams of sensory data (Infrared and vision based tracking results) are combined by a pose estimation algorithm based on RANSAC (RANDOM Sample Consensus) which is an iterative parameter estimation algorithm. Simulations of this work were performed on an artificially textured cube as a reference model.

3.2 Methods

For an AR system to be useful in a clinical context, it must be readily available and not provide a significant change to the existing workflow [8]. It is therefore important that the pre-processing required to prepare and segment medical images for use in AR systems is relatively rapid and uncomplicated [9]. Additionally, for our application to be suitable for use in the intensive care unit, it must be portable and requiring minimal setup. These are all of the requirements that affect the design of our system. In section 3.1 we discuss the use of image-based tracking through the Vuforia software development kit. In section 3.2, the design and implementation of the pipeline for importing patient-specific data is described. Section 3.3 covers the user interface design and section 3.4 describes our pilot evaluation of system accuracy.

3.2.1 Vuforia and Augmented Reality Implementation

AR can provide users with additional visuospatial context by overlaying anatomical images on the head of the patient. This can be beneficial to surgical planning and navigation by offering additional contextual information to a procedure through incorporation of preoperative medical imaging data. This gives surgeons the ability to not only view patient anatomy extracted from medical images, but to do so with spatial context relevant to the tasks performed during the procedure. The placement of an external ventricular drain requires surgeons to estimate entry points and trajectory paths relying on preoperative medical images and experience. Our AR tool allows surgeons to visualize – using a mobile device as a viewport - the location of internal anatomical features projected onto the patient. This provides the surgeon with additional contextual information to aid in navigational tasks with the intent of increasing accuracy compared to blind navigation.

The implementation of our application included the use of an AR software development kit, Vuforia, developed by Qualcomm [10]. The essential requirement of our system was the ability to register the three-dimensional virtual image-space to the physical world's three-dimensional space utilizing image-based marker tracking through a single on-board device camera. Qualcomm delivers an API capable of tracking multiple planar images using the mobile device's camera. For our application we constructed a 40mm x 60 mm x 80 mm rectangular cuboid shaped tracking object and printed unique, feature-rich, images on each of its six faces. Using Vuforia's API, the approximate pose of each of the detectable image faces were averaged and used as an approximate pose transformation for the entire tracker geometry. The tracker was attached to a pair of safety glasses that would be placed on the patient, as illustrated in Figure 3-1. We made the assumption that when the glasses rested on the patients head, they will rest directly on the nasion – the region between the frontal bone of the skull and nasal bones, which is easily discernable in CT images and exhibits high reproducibility among experts [11]. In this case, the tracker would be 5mm anterior to the patient's nasion, providing a landmark relative to the tracker. Using OpenGL ES, surface representations of the patient's segmented anatomy extracted from the CT images could be then be displayed to the user through the device's viewport.

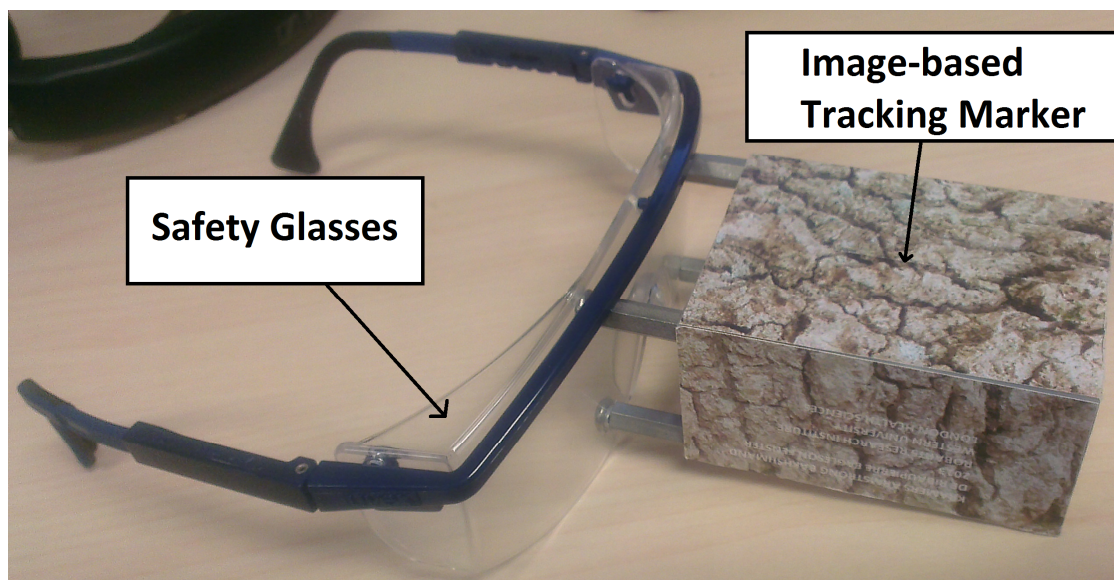


Figure 3-1: Tracking marker fixed to safety glasses for patient head pose estimation and registration of anatomy to scene.

An additional feature that was implemented was a second tracking device that could be used as a stylus within the augmented environment. This enables the user to view entry point trajectories with respect to the projected anatomy. In addition, this feature may provide cues to improve the user's depth perception by providing interaction with the objects in the scene. To achieve this, we rendered a virtual beam that emitted outwards from the pointing device towards the patient's head. This feature is depicted in Figure 3-2.

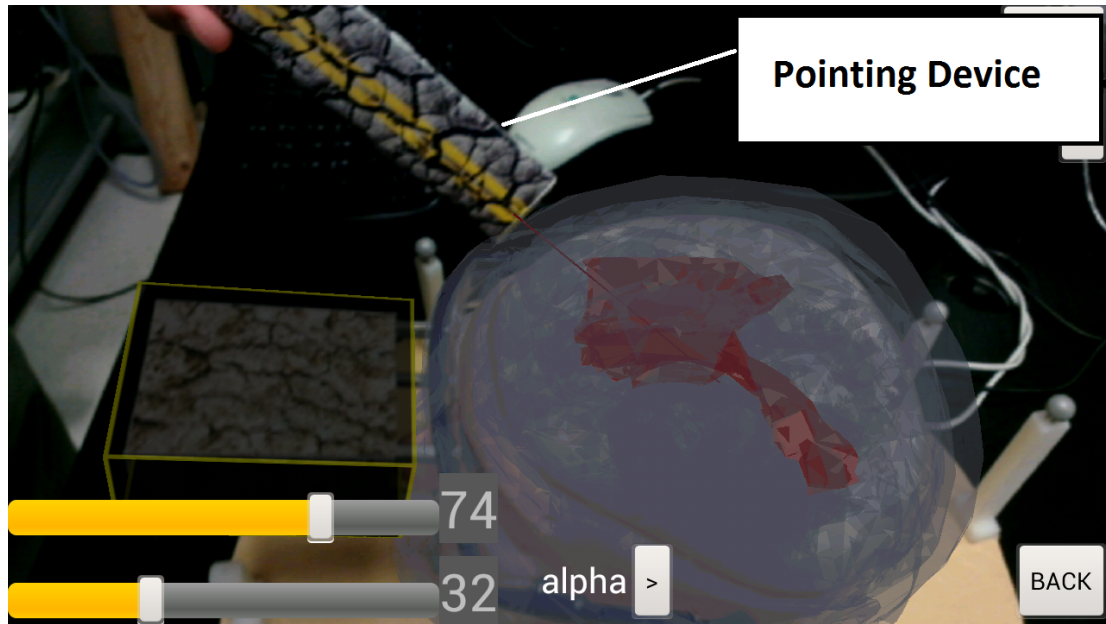


Figure 3-2: The tracked pointing device provides visual feedback for planning entry point locations and trajectories. The device also allows for additional interaction between the user and the AR scene.

The ability for a user to perceive the augmented surface graphics and gain contextual knowledge from the device depends on its ability to render graphics with appropriate visual cues for perceiving depth from 2D images. The skull surface, generated during the segmentation process, is used in the visualization with controlled blending to give the effect of being semi-transparent as the user views a patient's head through the device. By combining this visual element, texturing, shading, perspective projection, as well as the pointing stylus, an adequate viewport for ventricle navigation can be achieved.

3.2.2 Segmentation and Registration of Patient Data

In order to portray the internal anatomy of the patient overlaid in the scene, the anatomy of interest must first be segmented and registered into the scene. For these tasks, we have developed a custom interface to guide the user through such content creation. The software pipeline is modeled as a

wizard-style application that runs the user through the stages required to create all of the content, prompting for appropriate input when required. As we are targeting a neurosurgical procedure that is performed as an emergency, CT images will primarily be the imaging modality of choice preoperatively and thus, will serve as the input to our pipeline (contrasting with MR images that are done when the patient is stable). There are two anatomical features that are essential in our guidance system: the lateral ventricles to guide proper positioning of the EVD, and the outer skin of the head to visually verify alignment of the virtual and physical scenes. The outer skin segmentation can be performed automatically by selecting the entire outer boundary voxels of the input image. Segmentation of the lateral ventricles is less trivial due to strong inter-patient variation that occurs as a result of hydrocephalus and/or head trauma, as well as artifacts inherent to the preoperative images such as image noise, intensity inhomogeneity, low contrast and the resulting partial-volume effect. While there are automatic algorithms for segmentation of the lateral ventricles from CT images [12-14], the majority of these rely on prototypical model priors and are not robust when dealing with strong anatomical variations in the ventricular system. Additionally, while numerous segmentation platforms exist for semi-automatic extraction of features [15, 16], such platforms require algorithmic domain knowledge to achieve appropriate segmentations by fine-tuning parameters of the algorithm. As such, we have developed our pipeline as a standalone platform for ease of use by non-experts. In order to achieve an optimal balance of pipeline efficiency and segmentation accuracy, our approach employs a semi-automatic algorithm that relies on user knowledge and interaction. A recent survey [17] of semi-automatic techniques applied to segmentation of hydrocephalic ventricles indicated that the level set approach [18] was most effective compared to random walk [19] and min-cut/max-flow [20] algorithms. For maximum user efficiency, the level set algorithm is incorporated in our pipeline with the addition of a knowledge-

based region growing approach for initiation. Initially, the user must select two rectangular regions that correspond to each lateral ventricle, allowing placement of initial region growing seed points in image space as well as determination of image characteristics, such as noise. This allows fine-tuning of the algorithms without user intervention. When the segmentation of both lateral ventricles is complete, they are merged as we are only concerned about the general spatial features of the lateral ventricles, so leakage between them is of no concern.

After the segmentation, the user must verify that the ventricles were correctly segmented by examining either the raw image slices with the segmentation overlaid, or a volumetric rendering of the ventricles. The volumetric rendering module was developed to aid in quick verification of segmentation by emphasizing strong variations in intensity values of the segmented region, which are generally indicative of a region growing leak. When the user is satisfied with a given segmentation, a marching cubes [21] algorithm is performed on the volume and meshes of the ventricles and head are extracted. These meshes are further smoothed and decimated to achieve suitable performance on mobile devices. The amount of decimation will depend on the amount of video memory available.

Once the segmentation is complete, the coordinate system of the image space must be registered to the application's virtual space to ensure proper correspondence between the rendered ventricles in the display with the patient's head. To simplify this process, we make the assumption that the rectangular prism image-based marker is aligned perfectly with the patient's head. With orientation known, only position and scale of the anatomy must be determined. Scale is determined by saving a mapping from image space (where voxel millimeter spacing is known) to virtual space in relation to vertices in the scene. The relation of physical space to virtual space is determined by the tracking system since the dimensions of the image-based

marker are known. This allows proper scaling of the anatomy. Position is determined by prompting the user to select the point in the initial CT image that corresponds to the nasion. From the nasion, we know the distance to the center point on the attached side of the marker, allowing positioning of the anatomy at the appropriate location. The registration is depicted in Figure 3-3.

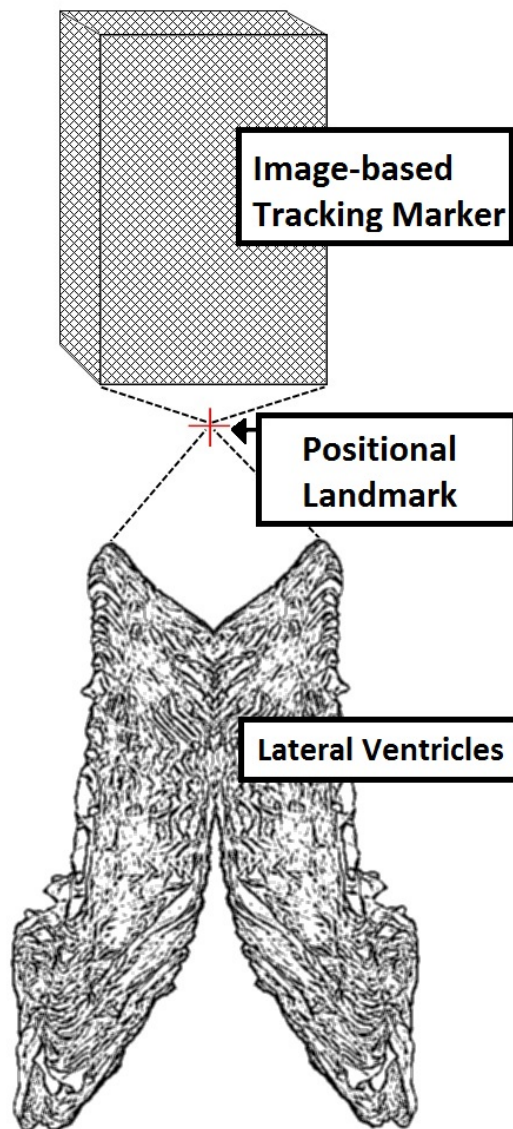


Figure 3-3: Anatomy segmented from preoperative images aligns with the physical tracker and is positioned using the nasion as a positional landmark.

3.2.3 User Controlled Registration Correction

Although the segmented surfaces were registered to several points on the patients head chosen during segmentation, an accurate placement of the tracking glasses cannot always be achievable. This can be caused by a number of factors, such as nose and head shape variations. For this reason, a user interface was developed to allow users to make adjustments to the alignment of the physical and virtual scenes. The user is able to manipulate the pose of the virtual space through translation, rotation and scaling controls using the skull as a reference as it is superimposed over the view of the patients head. This is illustrated in Figure 3-4. This allows the surgeon to visually correct misalignment due to improper or abnormal placement of the head-mounted marker or inaccurate placement of landmarks during scene generation.

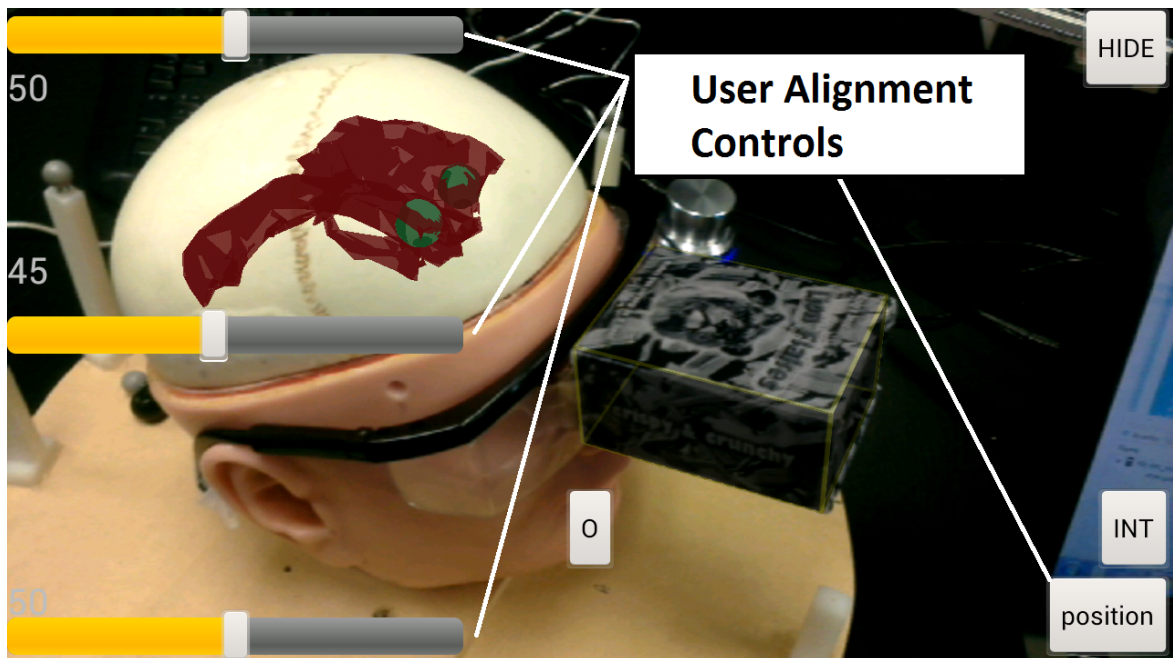


Figure 3-4: Users have access to multiple sliders and buttons to manually adjust the virtual models to achieve appropriate alignment of anatomy, as well as visual settings that aid in guidance.

3.2.4 **Evaluation of System Accuracy**

To evaluate the accuracy of our system, we performed a pilot study to quantify accuracy of the system applied to an environment of similar scale to the implementation. Our evaluation focused on system accuracy rather than user performance which will be evaluated in future work.

Accuracy was assessed by having users target corners of two-dimensional shapes projected onto a plane with known coordinates. A sheet of paper represented the plane in physical space, which was registered to the virtual plane. Rectangles and triangles were used as the shapes projected onto the plane as they offer clearly distinguishable corners for localization. The shapes were rendered transparently as to not impede the localization of points by the user.

As this is a pilot study to initially assess system accuracy, the study was limited to two users performing targeting tasks. The tasks required the user to place markers at the location that they perceived as the corners of the shapes as they were displayed to them. In addition, the virtual plane with targets was displayed on an external monitor so that the user had exposure to the position and shape of each target, prior to and during the targeting task. Since only accuracy was being evaluated, no constraints on time were imposed. The tasks were performed on a total of 10 shapes per user, with half of the tasks being guided by our augmented reality device, while the remaining tasks required users to rely only on the external monitor for reference. Analysis involved examining the deviation of the points on the physical plane placed by the user to their known positions on the plane in the virtual space.

3.3 Results

The Euclidean distance between each of the users' points and the virtual targets were calculated to determine targeting error. With AR guidance, the mean error for targeting was 9.88 ± 5.34 mm over a total of 35 individual points. When users did not have AR guidance, the mean error rose to 13.03 ± 6.15 mm, again over 35 individual points. To test the significance of this result, a Student's t-test was performed on both series of errors. The test indicated that the error when using AR guidance was significantly lower ($p < 0.05$) than the error without guidance. This result implies that our system may provide users with increased targeting accuracy compared to non-guided tasks.

Table 3-1: Targeting error measured as the Euclidean distance between targeted corner location and actual corner location

	No AR Guidance	AR Guided
Mean Error [mm]	13.04	9.88
Standard Deviation [mm]	6.15	5.34
P Value	0.0126	

3.4 Discussion

We have presented an application of AR for image guidance in emergency neurosurgical procedures. We focused on requirements of portability, ease of use, and cost efficiency to deliver an implementation that is suitable for use in intensive care unit interventions, particularly for placement of an EVD for treatment of hydrocephalus. Evaluations of the user interface will follow in future studies. An initial pilot studied examined the accuracy of the system, as well as offered insight into accuracy compared to non-guided tasks. Initial results look promising, but more evaluation must take place to further characterize the accuracy of the system, particularly with a focus on clinical relevance. Future work will involve assessing user driven segmentation, the

alignment of anatomical features internal to the head, and targeting and navigational performance for neurosurgical tasks augmented with the system. Additionally, future work will involve incorporating algorithms to account for the possibility of brain shift, offsetting the position of key anatomy at the time of surgery as well as examining variation in position of the patient-mounted tracker.

3.5 **Conclusion**

Effectively inserting an external ventricular shunt is a surgical task that relies heavily on the spatial relationships of neuroanatomical features and the surgeon's ability to recognize such relationships. Preoperative planning is essential to proper navigation, but operating surgeons must still rely on their spatial reasoning skills to perform the task blindly, increasing cognitive load. We have developed an AR application for mobile deployment in intensive care units for image guided shunt placement and performed a pilot assessment of the system's accuracy. Our results indicate that the accuracy of the system is in the range of a few millimeters, but such data is largely inconsequential in the absence of clinically defined thresholds and performance standards. As such, future work will determine the feasibility of the application for use in the clinic, as well as provide performance feedback to fine-tune the implementation and potentially validate its use compared to blind navigation.

3.6 **Acknowledgment**

We would like to acknowledge our sources of funding: GRAND NCE, NSERC, and the CAMI CREATE program. We also acknowledge Kevin Barker of Robarts Research Institute for help constructing the tracking glasses.

References

1. I. E. Sutherland, Proceedings of the December 9-11, 1968, fall joint computer conference, part I, 1968.

2. M. Bajura, H. Fuchs and R. Ohbuchi, ACM SIGGRAPH Computer Graphics, 1992.
3. R. R. Shamir, M. Horn, T. Blum, J.-H. Mehrkens, Y. Shoshan, L. Joskowicz and N. Navab, Biomedical Imaging: From Nano to Macro, 2011 IEEE International Symposium on, 2011.
4. R. Shamir, L. Joskowicz and Y. Shoshan, 5th International Symposium on Robotics and Automation, 2006.
5. R. A. Kockro, Y. T. Tsai, I. Ng, P. Hwang, C. Zhu, K. Agusanto, L. X. Hong and L. Serra, "Dex-Ray: Augmented Reality Neurosurgical Navigation With A Handheld Video Probe," *Neurosurgery* **65**, 795-808 (2009).
6. R. A. Mischkowski, M. J. Zinser, A. C. Kübler, B. Krug, U. Seifert and J. E. Zöller, "Application of an augmented reality tool for maxillary positioning in orthognathic surgery—a feasibility study," *Journal of Cranio-Maxillofacial Surgery* **34**, 478-483 (2006).
7. J. Fischer, M. Eichler, D. Bartz and W. Straßer, Proceedings of the 12th Eurographics conference on Virtual Environments, 2006.
8. L. J. Williams, "Tunnel vision induced by a foveal load manipulation," *Human Factors: The Journal of the Human Factors and Ergonomics Society* **27**, 221-227 (1985).
9. M. Lerotic, A. J. Chung, G. Mylonas and G.-Z. Yang, "Pq-space based non-photorealistic rendering for augmented reality," in *Medical Image Computing and Computer-Assisted Intervention—MICCAI 2007*, (Springer, 2007), pp. 102-109.
10. Qualcomm, "Vuforia Developer Portal," *Vol. 2013*, (2013), pp. Vuforia Developer Portal Website.
11. A. Muramatsu, H. Nawa, M. Kimura, K. Yoshida, M. Maeda, A. Katsumata, E. Arijii and S. Goto, "Reproducibility of maxillofacial anatomic landmarks on 3-dimensional computed tomographic images determined with the 95% confidence ellipse method," *The Angle Orthodontist* **78**, 396-402 (2008).
12. W. Chen, R. Smith, S.-Y. Ji and K. van Najarian, Bioinformatics and Biomeidcine Workshops, 2008. BIBMW 2008. IEEE International Conference on, 2008.
13. W. Chen, R. Smith, S.-Y. Ji, K. R. Ward and K. Najarian, "Automated ventricular systems segmentation in brain CT images by combining low-level segmentation and high-level template matching," *BMC medical informatics and decision making* **9**, S4 (2009).
14. J. Liu, S. Huang, V. Ihar, W. Ambrosius, L. C. Lee and W. L. Nowinski, "Automatic model-guided segmentation of the human brain ventricular system from CT images," *Academic radiology* **17**, 718-726 (2010).

15. P. A. Yushkevich, J. Piven, H. C. Hazlett, R. G. Smith, S. Ho, J. C. Gee and G. Gerig, "User-guided 3D active contour segmentation of anatomical structures: significantly improved efficiency and reliability," *Neuroimage* **31**, 1116-1128 (2006).
16. S. Pieper, M. Halle and R. Kikinis, *Biomedical Imaging: Nano to Macro*, 2004. IEEE International Symposium on, 2004.
17. T. Węgliński and A. Fabijańska, "Survey of Modern Image Segmentation Algorithms on CT Scans of Hydrocephalic Brains," *Image Processing & Communications* **17**, 223-230 (2012).
18. S. Osher and J. A. Sethian, "Fronts propagating with curvature-dependent speed: algorithms based on Hamilton-Jacobi formulations," *Journal of computational physics* **79**, 12-49 (1988).
19. L. Grady, "Random walks for image segmentation," *Pattern Analysis and Machine Intelligence, IEEE Transactions on* **28**, 1768-1783 (2006).
20. Y. Y. Boykov and M.-P. Jolly, *Computer Vision, 2001. ICCV 2001. Proceedings. Eighth IEEE International Conference on*, 2001.
21. W. E. Lorensen and H. E. Cline, *ACM Siggraph Computer Graphics*, 1987.

Chapter 4

4. Evaluation of a Mobile Augmented Reality Application for Image Guidance of Neurosurgical Interventions[†]

4.1 Introduction

The placement of an external ventricular drain (EVD) is a common neurosurgical procedure performed to treat hydrocephalus[1]. The procedure involves identifying an entry point on a patient's skull to place a burr-hole and thereby gain access to the ventricular system. Unlike many neurosurgical procedures, the placement of an EVD is often performed at a patient's bedside using mobile tools, as there are difficulties imposed by the relocation of a patient to an operating room [2]. This procedure is also frequently performed 'freehand,' without technical assistance, relying only on the operating surgeon's spatial abilities to plan an optimal trajectory. For these reasons, navigational error is not uncommon, and may lead to repeated targeting attempts as well as unnecessary complications such as infection or haemorrhage [3]. To address these issues, we have prototyped a mobile device application that utilizes augmented reality (AR) to provide spatial context of a patient's inner-anatomy to a surgeon, intra-operatively, by incorporating segmented preoperative CT images.

4.2 Methods

Our guidance system consists of a mobile device as well as a pair of modified safety glasses (see Figure 4-1) that are placed on the patient during the

[†]. A version of this chapter (with the exception of section 4.6 Additional Experiments) has been published: Kramers, M, Armstrong R., Bakhshmand, S.M., Fenster A., de Ribaupierre S., Eagleson R.: Evaluation of a mobile augmented reality application for image guidance of neurosurgical interventions. *Studies in Health Technology and Informatics*. 2014; 196:204-8.

procedure. The glasses are far away from the surgical field and therefore do not need to be sterile.



Figure 4-1: Glasses with attached tracking marker

The mobile device utilizes the Vuforia software development kit, developed by Qualcomm [4], to achieve image-based tracking required for augmented reality. The glasses used in our system include a tracking box fixed to the frame. The tracking box contains unique planar images on each of its visible faces. The Vuforia Target Manager was used to define the geometric relationships between each of the faces on the tracking box, as well as to encode the images into the proper format required by the framework. Using the real-time pose information provided by Vuforia, surface models of anatomy can be overlaid on the displayed image stream at the appropriate geometric locations and visualized by the user through the device's display. In the case of EVD placement, the surgeon would use the device as a viewport to visualize a patient's ventricular system as demonstrated in Figure 4-2.

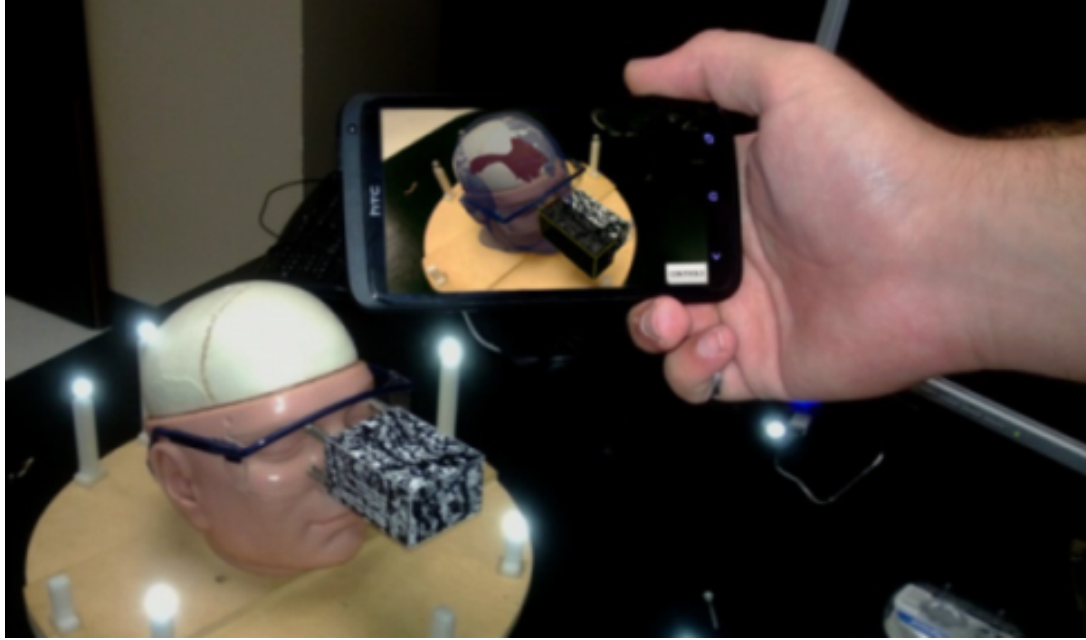


Figure 4-2: User viewing ventricular anatomy through device

Since at any point in time the display presents only monocular views, the user must control the viewpoint of the display in order to induce depth cues from motion parallax. Movement of the augmented display relative to the patient induces motion cues, providing additional depth information in the scene.

In order to compute the transformation between the tracked environment and the display, the system requires that a CT image of the patient's head be segmented, uploaded to the device, and registered within the augmented scene. In addition to the AR application, we have developed a user interface to perform the segmentation of a patient's ventricles and skull. Despite the availability of automated segmentation algorithms [5, 6] as well as semi-automated platforms [7, 8], we chose to create a semi-automatic tool that did not require the user to have knowledge of the underlying algorithms, thus simplifying the process for a wider audience of users. To ensure that the standard workflow is not significantly disrupted, the segmentation process simply requires the user to place rectangular regions around the

corresponding lateral ventricles in the image. The user is also directed to localize three point-based landmarks for scene registration, located in proximity to the external auditory canal and the nasion. Upon user initialization of the segmentation, the algorithm first employs a region growing algorithm as an initialization stage for a level set segmentation of the ventricles. This choice reflects the findings of a recent survey [9] of semi-automatic segmentation techniques applied to ventricles, which suggests that the level set approach [10] was most effective compared to random walk [11] and min-cut/max-flow [12] algorithms. This process then generates a surface mesh for the combined ventricles as well as the skull using the marching cubes algorithm [13]; both of which are rendered during the operation of the device. When the tracking glasses are placed on the patient, the arch of the glasses rests approximately on the patient's nasion – the region on the skull between the frontal bone and nasal bones, and the branches rest on the patient's ears. The glasses are adaptable to any head shape. Using the landmarks defined during the pre-processing stage, a registration of the virtual anatomy within the augmented scene can be performed. Since accurate placement of the glasses is subject to variability, the application provides an interface for manual adjustment of the scene registration. This allows the user to align the skull surface rendering visually with the patient's skull during operation, thus alleviating any scene misalignment caused from improper tracker positioning.

4.3 **Evaluation**

To assess the system's ability to provide consistent visuospatial context to a user, a series of five pilot experiments were conducted. In each experiment, users were required to perform pointing tasks on a physical head-phantom using a Polhemus Patriot electromagnetically tracked stylus.

In the first two experiments, users were required to localize the four corners of rectangular plane using the stylus a total of five times each. In the first set of tasks (Experiment #1), users performed the task without the AR device. Users then proceeded to perform the same task while looking through the device's viewport (Experiment #2). Both the position of the tip of the stylus was measured at each location along with the elapsed pointing time for each task. In the third experiment, a triangle was augmented within the scene. Users were required to localize each of the three corners of the triangle while stylus tip location and pointing time were recorded. In the final two experiments, a total of eight spherical landmarks were augmented onto the surface of the head phantom at various locations. Users were required to use the device to visualize and then localize each target. This was repeated a total of five times per target per user. In Experiment #4, the user was only able to visualize the targets projected onto the head. In Experiment #5, a texture was applied to the entire surface of the head phantom. By measuring the location of the stylus tip as well as pointing time, an evaluation of user variability could be achieved.

4.4 Results

Each experiment was performed a total of five times by a group of six participants, including one experienced neurosurgeon. The experiments focused on inter- and intra- user variability for performing pointing tasks while using the device. Summaries of the observed results are shown in Table 4-1 – 4-3.

Table 4-1: Average Intra-User Deviation from Target [mm]

Expt. #	User 1	User 2	User 3	User 4	User 5	User 6	Avg.	Std. Dev
1	1.01	3.36	1.04	0.99	0.99	2.06	1.57	0.97
2	2.67	2.95	2.19	2.24	3.61	3.36	2.84	0.58
3	1.36	2.73	1.72	1.55	1.38	1.93	1.78	0.51
4	5.12	5.54	6.92	4.39	3.30	8.09	5.56	1.73

5	4.50	6.53	3.82	7.73	5.03	6.39	5.67	1.46
---	------	------	------	------	------	------	------	------

Table 4-2: Average Inter-User Deviation from Target [mm]

Expt. #	User 1	User 2	User 3	User 4	User 5	User 6	Avg.	Std. Dev.
1	7.31	10.31	2.79	4.77	7.42	3.30	5.98	2.88
2	6.11	6.43	5.82	4.60	9.81	3.45	6.04	2.15
3	7.18	11.83	6.86	9.03	9.26	6.70	8.48	1.98
4	7.59	10.22	10.48	8.97	9.63	12.31	9.87	1.58
5	9.76	8.09	14.01	9.22	6.87	11.05	9.83	2.50

Table 4-3: Average pointing time [s]

Expt. #	User 1	User 2	User 3	User 4	User 5	User 6	Avg.	Std. Dev.
1	2.07	4.29	2.79	2.93	3.11	3.51	3.12	0.74
2	4.17	7.39	5.32	5.17	5.52	4.58	5.36	1.12
3	4.21	7.31	3.88	4.97	4.78	2.65	4.63	1.55
4	6.57	13.76	9.23	6.69	6.57	7.60	8.40	2.82
5	4.93	8.02	8.14	6.88	7.89	7.35	7.20	1.21

The results shown indicate that users were able to perform tasks consistently based on their perception of where each target was within the augmented scene. The difference between users (Table 4-2) was larger, which we suggest was caused by the slight misalignment of the tracking system with the AR device between trials. The average pointing time demonstrates the increased task time that arises when using the AR device, along with the increased standard error, thus quantifying the small incremental cost of using the ‘Augmented Reality’ device when compared with ‘Reality’.

4.5 Conclusion

We have presented an augmented reality application for mobile devices that provides image-guidance for neurosurgical tasks, specifically the placement of an external ventricular drain. The goal of the application was to improve a surgeon’s ability to perform three dimensional targeting tasks. A method for the evaluation of the system has been outlined and presented in detail. Pilot study results indicate that users can perform targeting tasks consistently

while using the device. The methodology developed here can be used to evaluate user performance for targeting tasks involving hand-held Augmented Reality displays. The small decrease in pointing accuracy provides a baseline with which to compare the future addition of augmenting the view with additional information such as pre-operative anatomical structures.

References

1. J. A. Kusske, P. T. Turner, G. A. Ojemann and A. B. Harris, "Ventriculostomy for the treatment of acute hydrocephalus following subarachnoid hemorrhage," *Journal of neurosurgery* **38**, 591-595 (1973).
2. P. Ferdinande, "Recommendations for intra-hospital transport of the severely head injured patient," *Intensive care medicine* **25**, 1441-1443 (1999).
3. A. Saladino, J. B. White, E. F. Wijdicks and G. Lanzino, "Malplacement of ventricular catheters by neurosurgeons: a single institution experience," *Neurocritical care* **10**, 248-252 (2009).
4. Qualcomm, "Vuforia Developer Portal," *Vol. 2013*, (2013), pp. Vuforia Developer Portal Website.
5. W. Chen, R. Smith, S.-Y. Ji, K. R. Ward and K. Najarian, "Automated ventricular systems segmentation in brain CT images by combining low-level segmentation and high-level template matching," *BMC medical informatics and decision making* **9**, S4 (2009).
6. R. A. Kockro, Y. T. Tsai, I. Ng, P. Hwang, C. Zhu, K. Agusanto, L. X. Hong and L. Serra, "Dex-Ray: Augmented Reality Neurosurgical Navigation With A Handheld Video Probe," *Neurosurgery* **65**, 795-808 (2009).
7. P. A. Yushkevich, J. Piven, H. C. Hazlett, R. G. Smith, S. Ho, J. C. Gee and G. Gerig, "User-guided 3D active contour segmentation of anatomical structures: significantly improved efficiency and reliability," *Neuroimage* **31**, 1116-1128 (2006).
8. S. Pieper, M. Halle and R. Kikinis, *Biomedical Imaging: Nano to Macro*, 2004. IEEE International Symposium on, 2004.
9. T. Węgliński and A. Fabijańska, "Survey of Modern Image Segmentation Algorithms on CT Scans of Hydrocephalic Brains," *Image Processing & Communications* **17**, 223-230 (2012).

10. S. Osher and J. A. Sethian, "Fronts propagating with curvature-dependent speed: algorithms based on Hamilton-Jacobi formulations," *Journal of computational physics* **79**, 12-49 (1988).
11. L. Grady, "Random walks for image segmentation," *Pattern Analysis and Machine Intelligence, IEEE Transactions on* **28**, 1768-1783 (2006).
12. Y. Y. Boykov and M.-P. Jolly, *Computer Vision, 2001. ICCV 2001. Proceedings. Eighth IEEE International Conference on*, 2001.
13. W. E. Lorensen and H. E. Cline, *ACM Siggraph Computer Graphics*, 1987.

Chapter 5

5. Conclusion

The work presented in this thesis was focused on developing and validating a methodology to evaluate human performance for image-guided surgical tasks. Two different interventional procedures that employ image-guidance devices were evaluated; the TRUS-guided prostate biopsy and external ventricular drain insertion, however the methodology discussed can be easily applied to a wide range of surgical and interventional procedures that rely on image guidance systems, including percutaneous procedures as well as other tasks related to targeting. Our work is based on the Fitts' Law methodology, which respects the speed-accuracy trade-off observable in human targeting tasks. It is important to note that although in many circumstances it may be desirable to place more focus on speed than accuracy, in surgery and interventional tasks, accuracy is typically the most important aspect of the task, especially when performing on human patients. Errors caused by user inaccuracies during a procedure can result in undesirable consequences to the patient, including tissue and organ damage leading to potential infection, as well as other potentially damaging side-effects. In this work, participants were advised to focus on both speed and accuracy equally such that optimal performance measurements could be observed and performance could be accurately quantified for a particular user performing a task. Our work focused more on the usability of image-guidance systems and devices than on the direct clinical outcome of the procedures the devices were designed for. Since new and unique image-guidance tools are constantly being developed and put into clinical practice, it is important to establish a standardized method for evaluating the human factors attributed with such devices, in this case, performance. Doing so effectively enables characteristics of such devices to be quantitatively evaluated with respect to user performance. In this work, we compared users to each other; however the same method could be applied

to compare system features such as visualization schemes, or device ergonomics and maneuverability. In addition, quantitative user performance information can also be useful for evaluating other related human factors associated with image-guidance systems; such as training strategies, learning curve evaluation, and proficiency testing. In general, we proposed and employed a method to collect human performance information for image-guided systems. This method can be applied in ways that enable the measurement of aforementioned human factor components of each system, and how users are introduced to, trained, and interact with the systems directly.

In summary, the TRUS-guided biopsy procedure and augmented reality guided external ventricular drain procedures were both analyzed, and user performance data was observed and collected for multiple users. Using techniques derived from the Fitts' Law methodology we were able to successfully determine and quantify an index of performance for each user. Using statistical evaluation methods we were able to confirm that the results collected throughout the study were significant, indicating that the methodology used was suitable for the purpose of evaluating human performance for these particular devices and the surgical procedures in general.

Appendix A: Additional Experiments

In addition to the targeting experiments performed in this work, an experiment was conducted to compare the performance of a novice user and an experienced neurosurgeon. Two users were instructed to perform trajectory estimation tasks by aligning an optically tracked stylus with virtual spherical targets placed within a head phantom. The users began the task by placing the stylus in a home position located at the parietal bone calvaria (top of the skull). Users then moved the stylus to a position and orientation on the surface of the skull such that the line projected from the long axis of the stylus intersected a virtual target within the lateral ventricle, representing the target location for EVD placement. The tasks were repeated a total of 50 each for both the left and right ventricle targets, alternating from left to right locations. The tasks were performed both blindly and with AR guidance provided by the mobile AR application. For blind tasks, users were shown the positions of the targets on an external monitor. In AR guided tasks, users viewed the head phantom through the mobile device, allowing the targets to be visualized within the head phantom. Error was measured as the minimum Euclidean distance between the line projected from the long axis of the stylus and the center of the target sphere. Time was recorded between the user beginning the task at the home position, and when the user pressed a footswitch upon satisfactory alignment of the stylus. The experimental setup is displayed in Figure A-1 below and the results are reported below in Table A-1.

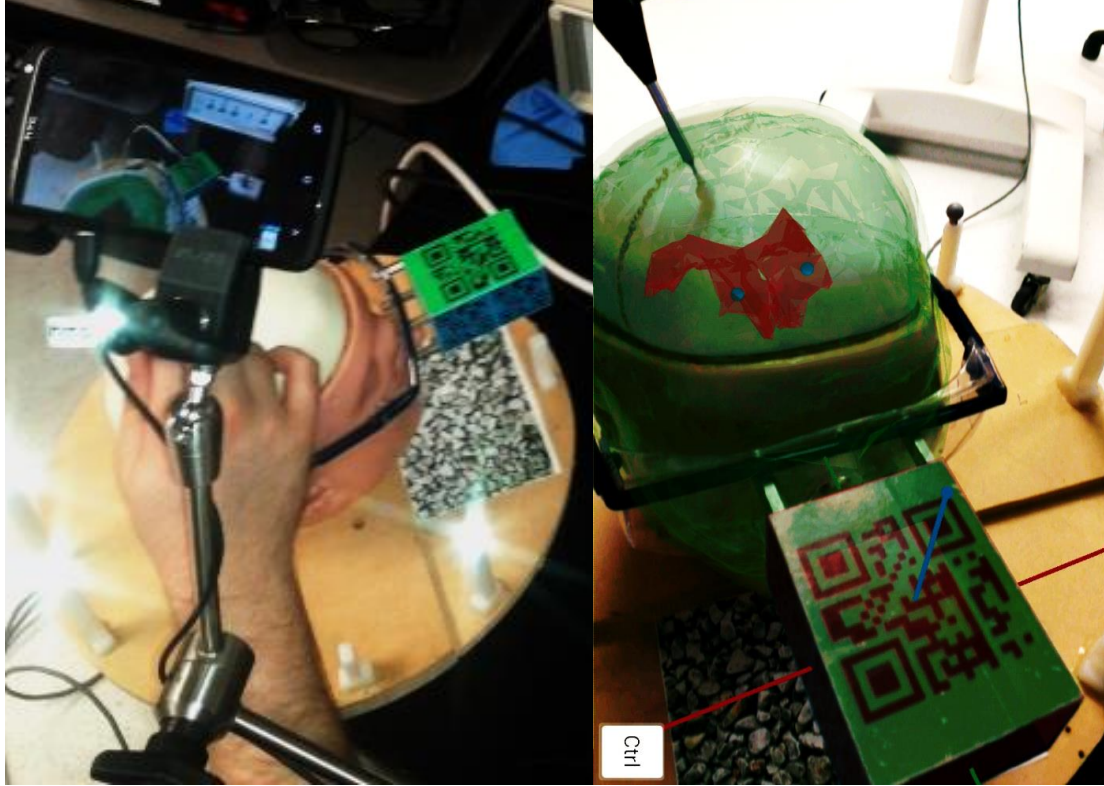


Figure A-1: Experimental setup for additional experiments described above

Table A-1: Experimental results for additional experiments comparing users of the mobile AR device

	Expert User			Novice User		
	Avg. Error [mm]	Std. Deviation [mm]	Avg. Pointing Time [ms]	Avg. Error [mm]	Std. Deviation [mm]	Avg. Pointing Time [ms]
Blind Targets	14.75	7.84	1046.04	24.20	9.96	1706.7
AR Guided Targets	14.03	8.48	1986.50	23.15	9.07	3113.69

Based on the observed results, the expert user performed the trajectory alignment tasks more accurately using both guidance methods and with lower standard deviation compared to the novice user. In addition, the expert user performed the tasks in less time on average. When comparing the

blindly guided tasks with the AR guided tasks, both users performed the tasks with lower error while using AR guidance, however the average pointing time increased as well. This may be indicative of the trade-off between speed and accuracy that users face when using the AR guidance device. In future work, additional users will be included in this study to allow for a more complete comparison of both experts versus novices, as well as the effect on performance while using the device when compared to blindly guided tasks.

Appendix B: Software Design and Architecture

A number of different software languages and development tools were used in this project. This section provides an overview of the software architecture and development details for both the TRUS-guided prostate biopsy interface and data collection program, and the augmented reality application.

TRUS-guided Prostate Biopsy Interface

The prostate biopsy device and the associated clinical software was originally designed in our lab prior to starting this project, however a number of major modifications were required to allow the software to generate and display custom targets to be displayed to the user and adequate user data to be collected during the experiments. Instead of modifying the existing software to fit our purpose, a new application was developed utilizing some of the existing components. The new application was developed using the C# language primarily with the Visual Studio 2012 [1] (Visual Studio 2013 was used in the later versions) integrated development environment. In addition to the standard .NET Windows Forms for user input via buttons, textboxes, and sliders, a managed version of Visualization Toolkit (VTK) [2] was used for the purpose of displaying graphics to the user. To establish a link between the software and the physical encoders on the device, the .NET serial communication functions were used (SerialPort class [3]). In addition to the existing hardware, a footswitch was modified to allow serial notification to the software from the user to progress the experiment. Using the .NET StreamWriter class [4], file logging functionality was incorporated into the application such that trajectory data (updating at approximately 100Hz), foot-press timing data, and user information could be stored for analysis. In order to provide continuous updating of the graphics as the user actuated the physical device, the BackgroundWorker class [5] was used to provide background updates of the VTK rendering window on a separate thread. This

allowed for user interaction to not have any effect on the rendering loop, ensuring that smooth visual feedback was provided to the user. The serial communication was performed using an event driven pipeline, for both the device encoders as well as footswitch. An Arduino [6] microcontroller was attached inline to the footswitch to allow for customized serial commands to be sent to the computer USB port when a foot press was detected. To ensure smooth operation, the footswitch signal was denounced and the character 'A' was sent over serial to ensure proper handling of the signal within the application. In order to transform the 4 device encoders' readings to needle tip position, the device's kinematics were evaluated, and then used to calculate the position for each iteration of the update loop. For testing and development purposes, three sliders were created using the Visual Studio Windows Forms [7] toolbox to emulate the encoders.

Augmented Reality Application

The augmented reality application utilized the Vuforia software development kit by Qualcomm to design an image cube for tracking as well as implement the tracking required to achieve augmented reality. The Vuforia API is called by the Android Native Development Kit (NDK) [8] which is based on the C++ language. The graphics that were overlaid (segmented later ventricle surface models) were visualized using OpenGL ES 2.0 [9] which can run on mobile Android devices. For all user interface components, Java was used along with the available widgets such as TextView [10] and SeekBar [11] to allow user interaction through sliders and text selection. All NDK calls were made from the Java application layer, allowing for native code (C++) to be run on top of the Java user interface layer. The Vuforia SDK provided all camera control and calibration components as well as visualization of camera images, which were then augmented with graphics. Using the online developer application, an image cube was created and then loaded into the application. The SDK provided functions that output the 3D transformation

matrix of the image cube when it was in view of the camera, and then functions were developed to display the overlaid graphics in the proper position and orientation with respect to the image cube. All development was performed using the Eclipse Integrated Development Environment [12].

In order to measure user performance with the device, the experimental setup used the NDI Polaris Infrared tracking system [13]. A stylus with spherical reflective markers was calibrated such that the position and orientation of the stylus tip could be calculated when in view of the tracking system. The development used a custom VTK class developed as part of the Atamai Image Guided Surgery Toolkit [14] that communicated with the tracking system, and allowed for the transformation matrix to be computed and used within the application. In addition, the head phantom also contained reflective spheres that were calibrated with the tracking system such that its position and orientation could be calculated and used as a reference position for the stylus. Using built-in VTK timer call-backs, the tracker was updated in real-time allowing the pose of the stylus to be calculated with respect to the head phantom in real-time. Targets were generated using VTK and placed both on the surface of the head phantom as well as within the head phantom for user targeting. The targets were exported using a custom application that converted VTK polydata into a header file that could be read and visualized by the Android application. A footswitch connected to an Arduino microcontroller was used to allow for the user to indicate that a target was successfully reached and to progress the experiment.

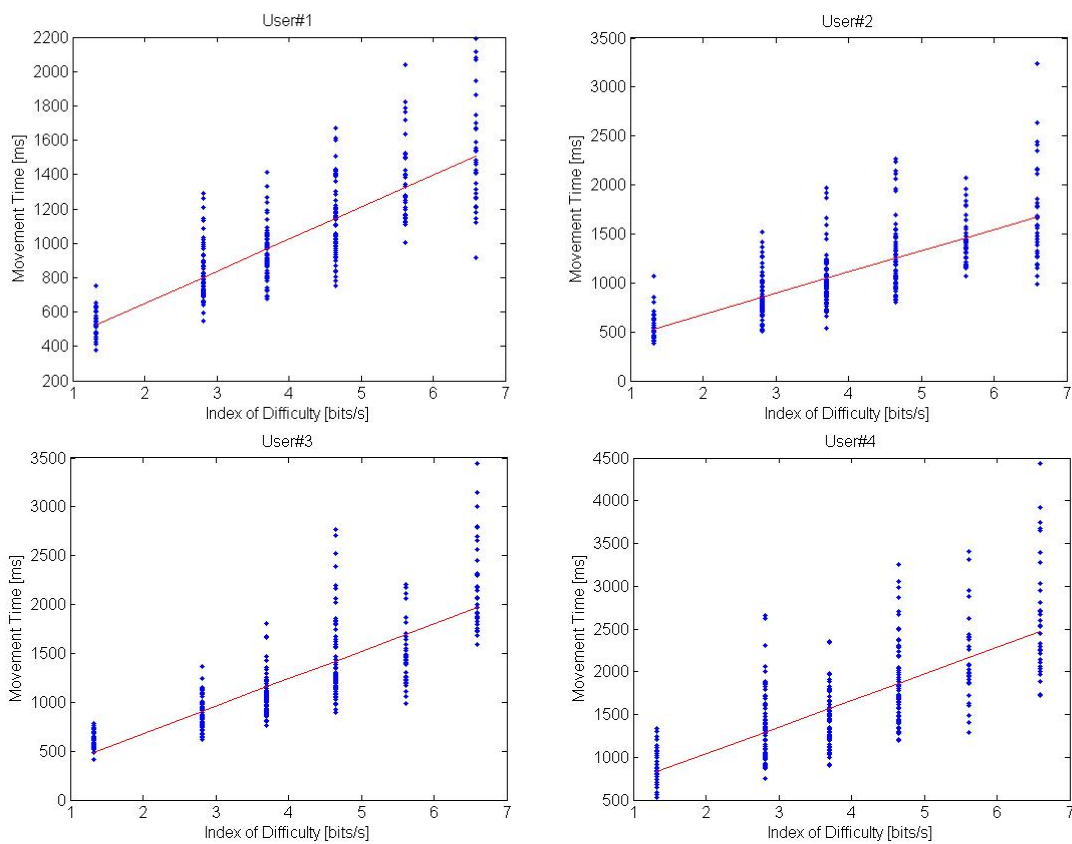
References

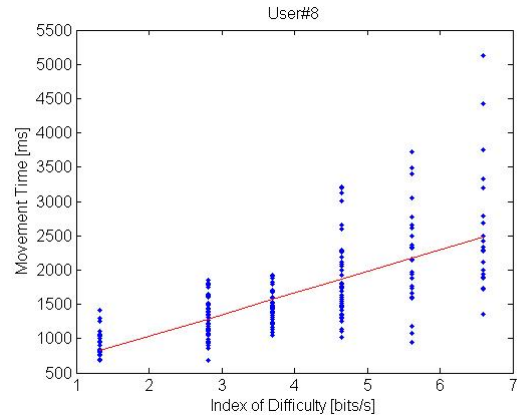
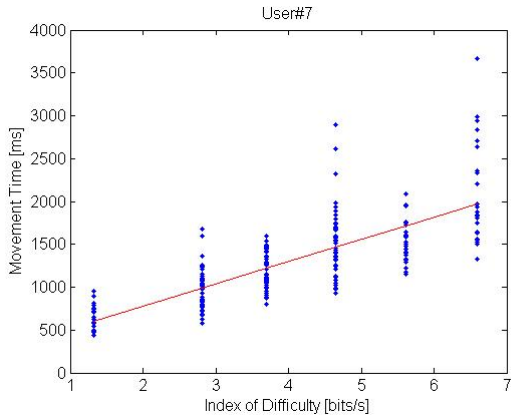
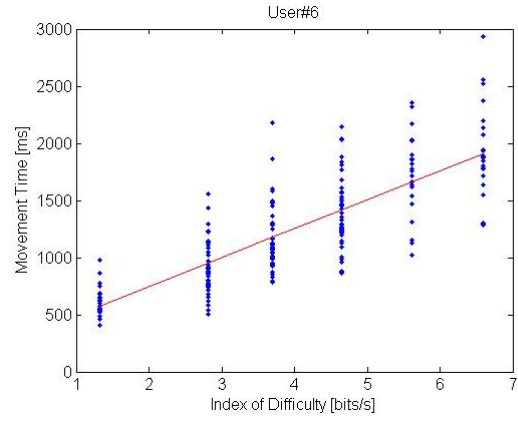
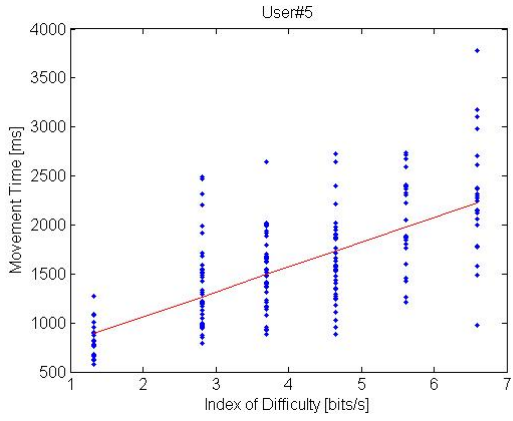
1. Microsoft Visual Studio. Retrieved Aug 8, 2014, from <http://msdn.microsoft.com/en-ca/vstudio/aa718325.aspx>
2. Visualization Toolkit. Retrieved Aug 8, 2014, from <http://www.vtk.org/>

3. SerialPort Class. Retrieved Aug 8, 2014, from [http://msdn.microsoft.com/en-us/library/system.io.ports.serialport\(v=vs.110\).aspx](http://msdn.microsoft.com/en-us/library/system.io.ports.serialport(v=vs.110).aspx)
4. StreamWriter Class. Retrieved Aug 8, 2014, from [http://msdn.microsoft.com/en-us/library/system.io.streamwriter\(v=vs.110\).aspx](http://msdn.microsoft.com/en-us/library/system.io.streamwriter(v=vs.110).aspx)
5. BackgroundWorker Class. Retrieved Aug 8, 2014, from [http://msdn.microsoft.com/en-us/library/system.componentmodel.backgroundworker\(v=vs.110\).aspx](http://msdn.microsoft.com/en-us/library/system.componentmodel.backgroundworker(v=vs.110).aspx)
6. Arduino. Retrieved Aug 8, 2014, from <http://www.arduino.cc/>
7. Windows Forms. Retrieved Aug 8, 2014, from [http://msdn.microsoft.com/en-us/library/dd30h2yb\(v=vs.110\).aspx](http://msdn.microsoft.com/en-us/library/dd30h2yb(v=vs.110).aspx)
8. Android Native Development Kit. Retrieved Aug 8, 2014, from <https://developer.android.com/tools/sdk/ndk/index.html>
9. OpenGL ES. Retrieved Aug 8, 2014, from <http://www.khronos.org/opengles/>
10. TextView | Android Developers. Retrieved Aug 8, 2014, from <http://developer.android.com/reference/android/widget/TextView.html>
11. Seekbar | Android Developers. Retrieved Aug 8, 2014, from <http://developer.android.com/reference/android/widget/SeekBar.html>
12. Eclipse. Retrieved Aug 8, 2014, from <https://www.eclipse.org/>
13. Medical Polaris Optical Tracking Systems. Retrieved Aug 8, 2014, from <http://www.ndigital.com/medical/products/polaris-family/>
14. Atamai Image Guided Surgery. Retrieved Aug 8, 2014, from <https://github.com/dgobbi/AIGS>

Appendix C: Supplementary Data

Table A-1: User performance data for guided prostate biopsy experiments for 8 users performed in Chapter 2





Appendix D: Supplementary Images

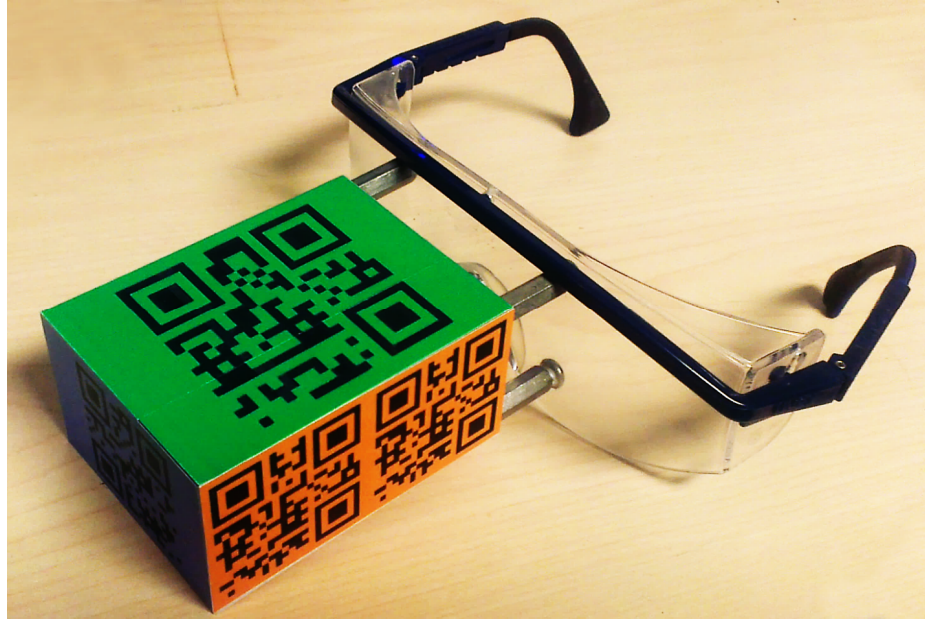


Figure B-1: Updated tracking glasses used for mobile AR application

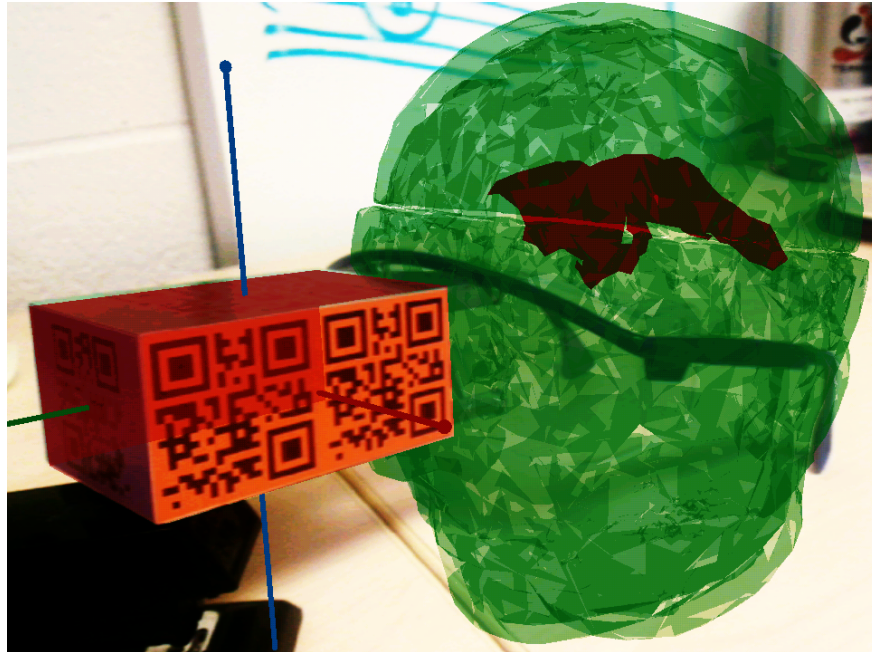


Figure B-2: Demonstration of AR visualization where the surface of the head phantom is rendered using alpha blending, and ventricle surface model are rendered to appear embedded within the skull

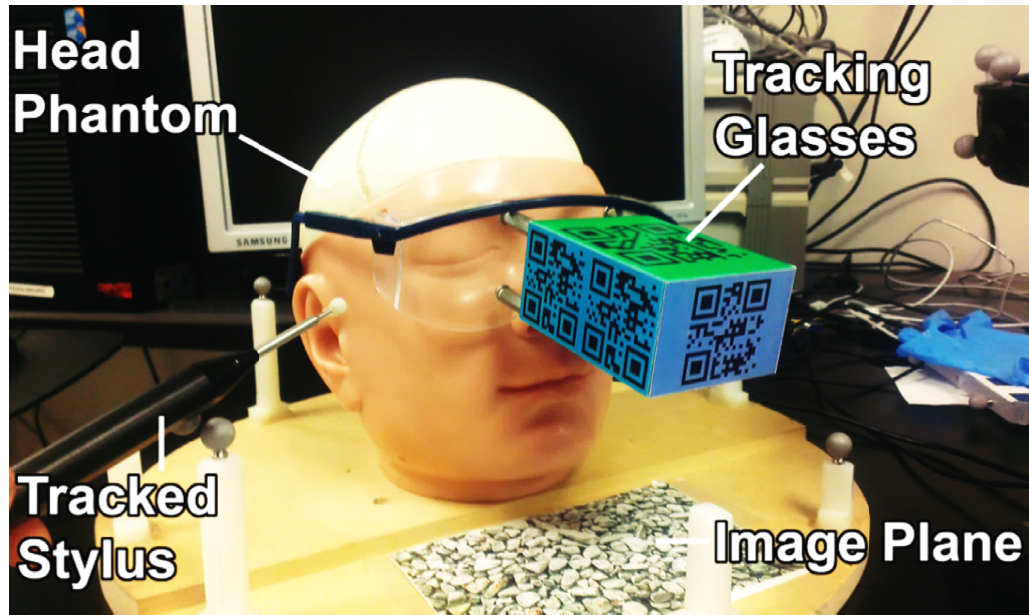


Figure B-3: Detailed image of experimental setup used in experiments described in Chapter 3 and 4

Appendix E: Permissions

Dear Matthew Kramers,

Thank you for your kind email.

Authors of content published in a SAP journal are permitted to reuse or reproduce portions of their publication in their own work, provided that the original source of the reproduced material is stated.

Best regards,

Evelyn Miller
Editorial Assistant
Scientific & Academic Publishing (<http://www.sapub.org/>), USA

Figure C-1: Permission to reproduce previously published material in Chapter 3.

Dear Matt Kramers,

We hereby grant you permission to reproduce the below mentioned material in **print and electronic format** at no charge subject to the following conditions:

1. If any part of the material to be used (for example, figures) has appeared in our publication with credit or acknowledgement to another source, permission must also be sought from that source. If such permission is not obtained then that material may not be included in your publication/copies.
2. Suitable acknowledgement to the source must be made, either as a footnote or in a reference list at the end of your publication, as follows:
"Reprinted from Publication title, Vol number, Author(s), Title of article, Pages No., Copyright (Year), with permission from IOS Press".
3. This permission is granted for non-exclusive world **English** rights only. For other languages please reapply separately for each one required.
4. Reproduction of this material is confined to the purpose for which permission is hereby given.

Yours sincerely

Carry Koolbergen (Mrs.)
Contracts, Rights & Permissions Coordinator

Figure C-2: Permission to reproduce previously published material in Chapter 4.

Curriculum Vitae

EDUCATION

- Sep. 2012 – **Master of Engineering Science**
ongoing Department of Biomedical Engineering
Western University, London, Canada
Supervisors: Dr. Roy Eagleson, Dr. Aaron Fenster
Thesis: “Evaluating Image-Guided Human Performance for Surgical Tasks”
- Sep. 2007 – **Bachelor of Engineering Science (Electrical)**
Apr. 2012 Department of Electrical Engineering
Western University, London, Canada
Senior Year Supervisor: Dr. Roy Eagleson
Senior Year Thesis: “Visualization and User Interface for Prostate Biopsy”

EMPLOYMENT

- Jan. 2014 – **Graduate Teaching Assistant**
present ECE4489b: “Computer Architecture Engineering”
Department of Electrical Engineering
Western University, London, Canada
Duties: Conducted detailed tutorials for students and assisted with projects and assignments in a laboratory setting
- Sept. 2014 – **Graduate Teaching Assistant**
Dec. 2014 ECE1036a: “Computer Programming Fundamentals”
Department of Engineering Sciences
Western University, London, Canada
Duties: Supervised engineering students in the laboratory and aided with troubleshooting of C++ computer programming projects
- Jan 2013 – **Graduate Teaching Assistant**
Apr. 2014 ECE2241b: “Electrical Circuits Laboratory II”
Department of Electrical Engineering
Western University, London, Canada
Duties: Supervised engineering students in the laboratory and aided with troubleshooting of electric circuits
- Sep. 2012 – **Graduate Teaching Assistant**

- Dec. 2012 ECE2240a: “Electrical Circuits Laboratory I”
 Department of Electrical Engineering
 Western University, London, Canada
Duties: Assisted students with construction, measurement and troubleshooting of electronic circuits
- May 2012 – **Research Assistant, Summer Research Assistantship**
 Aug. 2012 Robarts Research Institute, London, Canada
Supervisor: Dr. Aaron Fenster
Project: ”User-Interface Development for a Prostate Biopsy Device”
- May 2010 – **Electrical Engineering Intern**
 Aug. 2011 General Motors of Canada CAMI, Ingersoll, Ontario, Canada
Duties: Planned and implemented various electrical-based projects including assembly line equipment design and installation, facility lighting installations, and factory automation.
- May 2009 – **General Labourer**
 Sep. 2009 Excalibur Crossbow, Kitchener, Ontario, Canada
- May 2008 – **CNC Machine Operator**
 Sep. 2008 Anchor Edbar, Fergus, Ontario, Canada
- May 2007 – **CNC Machine Operator**
 Sep. 2007 Ready Precision, Guelph, Ontario, Canada

ACADEMIC AWARDS, SCHOLARSHIPS and DISTINCTIONS

- Sep. 2012 – **NSERC CREATE Computer Assisted Medical Interventions (CAMI)**
 present Western University, London, Canada
Awarded to graduate students pursuing research in the field of interventional surgery and therapy
 Institutional
Total Awarded: \$18,000
- Sep. 2012 – **Western Graduate Research Scholarship (WRGS)**
 present Western University, London, Canada
Awarded to a full time graduate student for stipend support who has maintained an average of 80% or more.
 Institutional
Total Awarded: \$14,664

- May 2012, **Dean's Honor List**
May 2009 Western University, London, Canada
Awarded to a full-time student who has maintained an average of 80% or more.
Institutional
- Nov. 2009 **Arthur S. Coveart Engineering Award**
Western University, London, Canada
Awarded to students in electrical engineering based on academic excellence.
Institutional
- Total Awarded: \$1400**

PUBLICATIONS, PRESENTATIONS and ABSTRACTS

A. Refereed Journal Publications (3)

Published (1)

1. **M Kramers**, R Armstrong, S Bakhsmand, A. Fenster, S de Ribaupierre, R Eagleson: *A Mobile Augmented Reality Application for Image Guidance of Neurosurgical Interventions*. American Journal of Biomedical Engineering 2013, 3(6): 169-174

In Preparation (1)

1. **M. Kramers**, S. de Ribaupierre, A. Fenster, R. Eagleson: *Evaluating Human Performance for Needle Guidance Tasks Using a Prostate Biopsy Device*
IEEE International Conference on Systems, Man, and Cybernetics 2014

B. Published Conference Proceedings (1)

1. **M Kramers**, R Armstrong, S Bakhsmand, A. Fenster, S de Ribaupierre, R Eagleson: *Evaluation of a Mobile Augmented Reality Application for Image Guidance of Neurosurgical Interventions*. NextMed/MMVR21 Medicine Meets Virtual Reality Conference Proceedings 2014, 192: 204-208

C. Selected Peer Reviewed Published Conference Abstracts (3)

1. **M. Kramers**, S. de Ribaupierre, A. Fenster, R. Eagleson: *Evaluating Image-guided Human Performance for Surgical tasks*. Computer Assisted Radiology and Surgery (CARS) 2014

2. **M. Kramers**, R Eagleson, R Armstrong, S Bakhsmand, A. Fenster, S de Ribaupierre: *Development of a Mobile Augmented Reality Device for Bed-side Guidance of EVD Insertion*. European Society for Pediatric Neurosurgery Congress 2014 (24th ESPN) 2014

3. **M. Kramers**, S. de Ribaupierre, A. Fenster, R. Eagleson: *Evaluation of a Mobile Augmented Reality Application for Image Guidance of Neurosurgical Interventions*. NextMed/MMVR21 Medicine Meets Virtual Reality 2014

D. Selected Peer Reviewed Poster Presentations (2)

1. **M. Kramers**, S. de Ribaupierre, A. Fenster, R. Eagleson: *Evaluating Image-guided Human Performance for Surgical tasks*. London Health Research Day 2014 (03/14)

2. **M. Kramers**, S. de Ribaupierre, A. Fenster, R. Eagleson: *Evaluation of a Mobile Augmented Reality Application for Image Guidance of Neurosurgical Interventions*. NextMed/MMVR21 Medicine Meets Virtual Reality 2014 (02/14)

POST-GRADUATE PROFESSIONAL DEVELOPMENT

Jan. 2014 **Practice Your Presentation Skills I, MITACS Step Program**

Instructor: Adam Lazarus

Objective To improve public speaking skills

Nov. 2013 **Imaging Applications in Prostate Cancer Workshop**

Objective Discuss research and development of prostate cancer diagnosis and treatment techniques

Feb. 2013 **Team Building Workshop, MITACS Step Program**

Instructor: Corey Atkinson

Objective: To enhance team building strategies through an interactive workshop

Sep. 2012 **Proactive and Practical Communication Workshop, MITACS Step Program**

Instructor: Corey Atkinson

Objective: To explore communication techniques using a wide array of

examples and demonstrations

RELEVANT ACADEMIC COURSES

Jan. 2013 - ongoing	BIOMED9515	Medical Mechatronics – 91%
Sept. 2013 – Dec. 2013	BIOMED9513	Introduction to Medical Imaging – 87%
Jan. 2013 –	BIOMED 9511	Image Guided Interventions – 88%
Apr. 2013	BIOMED 9550	Principles of Communication & Knowledge – 90%
Sept. 2012 –	BIOMED 9501	Biomedical Engineering I – 90%
Dec. 2012	BIOMED 9509	Introduction to Digital Image Processing – 93%
	VASCROG 9603	Research Ethics and Biostatistics – 93%
Sep. 2011 –	ECE 4416	Electrical Engineering Project – 90%
Apr. 2012	ECE 4429	Advanced Digital Signal Processing – 86%
	ECE 4460	Real-Time Embedded Systems – 90%
	ECE 4489	Computer Architectures – 90%
	ECE 4433	Digital Communication Systems – 93%
	ECE 4434	Advanced Digital Systems – 91%

LEADERSHIP & VOLUNTEER ACTIVITIES

2013 - 2014	Volunteer
	Engineering Intent to Register Information Session
	Western University

INTERESTS & QUALIFICATIONS

Software Design

Visualization Tools and Graphical User Interfaces

Programming Languages

C#, C++, Java, MATLAB, VisualBasic, Python, C, Assembly

Development Tools

VTK (Visualization Toolkit), .NET, CMake, OpenGL, OpenCV, Android SDK, Android NDK, Vuforia SDK, ITK, QT, Mono, NDI Libraries, MATLAB Image Processing Toolbox, Visual Studio, Eclipse, QT

Creator, Windows, Linux, Arduino IDE, Energia, CodeComposer
Studio

Microcontroller Programming and Home Automation

Raspberry Pi, Arduino, MSP430

Digital Audio Composition and Production

FL Studio